Available online at www.sciencedirect.com
ScienceDirect
Lithos 98 (2007) 67–96
LITHOS
www.elsevier.com/locate/lithos

Geochemical and Sr–Nd–Pb isotopic compositions of the Eocene Dölek and Sariçiçek Plutons, Eastern Turkey: Implications for magma interaction in the genesis of high-K calc-alkaline granitoids in a post-collision extensional setting

Orhan Karsli [a,*], Bin Chen [b], Faruk Aydin [c], Cüneyt Şen [d]

[a] Department of Geological Engineering, Karadeniz Technical University, TR-29000 Gümüşhane, Turkey
[b] School of Earth and Space Sciences, Peking University, 100871 Beijing, China
[c] Department of Geological Engineering, Niğde University, TR-51200 Niğde, Turkey
[d] Department of Geological Engineering, Karadeniz Technical University, TR-61080 Trabzon, Turkey

Received 13 June 2006; accepted 20 March 2007
Available online 1 April 2007

Abstract

The major and trace elements and Sr–Nd–Pb isotopes of the host rocks and the mafic microgranular enclaves (MME) gathered from the Dölek and Sariçiçek plutons, Eastern Turkey, were studied to understand the underlying petrogenesis and geodynamic setting. The plutons were emplaced at ~43 Ma at shallow depths (~5 to 9 km) as estimated from Al-in hornblende geobarometry. The host rocks consist of a variety of rock types ranging from diorite to granite (SiO_2=56.98–72.67 wt.%; Mg#=36.8–50.0) populated by MMEs of gabbroic diorite to monzodiorite in composition (SiO_2=53.21–60.94 wt.%; Mg#=44.4–53.5). All the rocks show a high-K calc-alkaline differentiation trend. Chondrite-normalized REE patterns are moderately fractionated and relatively flat [$(La/Yb)_N$=5.11 to 8.51]. They display small negative Eu anomalies (Eu/Eu*=0.62 to 0.88), with enrichment of LILE and depletion of HFSE. Initial Nd–Sr isotopic compositions for the host rocks are ε_{Nd}(43 Ma)=−0.6 to 0.8 and mostly I_{Sr}=0.70482–0.70548. The Nd model ages (T_{DM}) vary from 0.84 to 0.99 Ga. The Pb isotopic ratios are ($^{206}Pb/^{204}Pb$)=18.60–18.65, ($^{207}Pb/^{204}Pb$)=15.61–15.66 and ($^{208}Pb/^{204}Pb$)=38.69–38.85. Compared with the host rocks, the MMEs are relatively homogeneous in isotopic composition, with I_{Sr} ranging from 0.70485 to 0.70517, ε_{Nd}(43 Ma) −0.1 to 0.8 and with Pb isotopic ratios of ($^{206}Pb/^{204}Pb$)=18.58–18.64, ($^{207}Pb/^{204}Pb$)=15.60–15.66 and ($^{208}Pb/^{204}Pb$)=38.64–38.77. The MMEs have T_{DM} ranging from 0.86 to 1.36 Ga. The geochemical and isotopic similarities between the MMEs and their host rocks indicate that the enclaves are of mixed origin and are most probably formed by the interaction between the lower crust- and mantle-derived magmas. All the geochemical data, in conjunction with the geodynamic evidence, suggest that a basic magma derived from an enriched subcontinental lithospheric mantle, probably triggered by the upwelling of the asthenophere, and interacted with a crustal melt that originated from the dehydration melting of the mafic lower crust at deep crustal levels. Modeling based on the Sr–Nd isotope data indicates that ~77–83% of the subcontinental lithospheric mantle involved in the genesis. Consequently, the interaction process played an important role in the genesis of the hybrid granitoid bodies, which subsequently underwent a fractional crystallization process along with minor amounts of crustal assimilation, en route to the upper crustal levels generating a wide variety of rock types ranging from diorite to granite in an extensional regime.

Keywords: Eastern Turkey; Granitoid rocks; Magma interaction; Mafic microgranular enclave; Radiogenic isotopes

* Corresponding author.
E-mail address: okarsli@ktu.edu.tr (O. Karsli).

0024-4937/$ - see front matter © 2007 Elsevier B.V. All rights reserved.
doi:10.1016/j.lithos.2007.03.005

1. Introduction

As main components of the continental crust, granitoids are regarded as one of the key elements to understand the tectonics and geological evolution. They are genetically classified as peraluminous granitoids of crustal origin (e.g. Chappell and White, 1992; Chappell, 1999), alkaline granitoids of mantle origin (e.g. Turner et al., 1992; Han et al., 1997; Volkert et al., 2000) and calc-alkaline granitoids of mixed origin having various proportions of crust- and mantle-derived components (e.g. Poli and Tommasini, 1991; Barbarin and Didier, 1992; Wiebe, 1996; Altherr et al., 2000; Chen et al., 2002). It is likely that the latter represents a particular geological setting and provides greater information about the post-collisional magmatic processes in an extensional regime. Furthermore, the mafic–felsic interaction is an important part of the overall processes in calc-alkaline magmatism as revealed by rheological and geochemical data of coeval magmas (e.g. Barbarin and Didier, 1992; Wiebe, 1996) where the mafic components are represented by those MMEs within the host rocks (e.g. Vernon, 1990; Poli and Tommasini, 1991; Barbarin and Didier, 1992; Elburg, 1996). Therefore, they are commonly interpreted as magmatic precursors to interaction process and are regarded as potentially important tracer in understanding the hybrid calc-alkaline granitoid rocks. However, there are still some critical issues concerning the magma interaction that are open to debate: the petrogenetic processes responsible for the generation and chemical variation of the hybrid intermediate rocks, how the obstacles with chemical and physical origin that prevent the interaction of two distinct magmas are overcome at depth and the role and significance of MMEs that are commonly present in the hybrid magmas.

In the Eastern Pontides, several granitoid plutons were examined to identify the geodynamics of the region (e.g. Yilmaz, 1972; Yilmaz and Boztuğ, 1996; Okay and Şahintürk, 1997; Karsli et al., 2004a; Boztuğ et al., 2004; Topuz et al., 2005; Boztuğ et al., 2006; Dokuz et al., 2006), but little effort has been made to combine the tectonics and the petrological data in order to contribute to the understanding of the geodynamic evolution of the Eastern Pontides. The chemical, isotopic and geochronological data in the region are very limited. A wide spectrum of rock types from diorite to granite and MMEs are well exposed in the area that makes the Eocene Dölek and Sariçiçek plutons ideal candidates to evaluate the underlying processes of magma interaction. The current study aims to understand (i) the petrogenetic model responsible for the generation of young granitoid rocks and their source characteristics, (ii) origin of the MMEs, (iii) emplacement age of the plutons, and (iv) geodynamic setting of the plutons by the use of Sr–Nd–Pb isotopes, mineral and whole-rock chemical compositions and geochronological data.

2. Geological setting

Eastern Turkey is divided into five major tectonic blocks based on their geological and tectonic properties (Şengör et al., 2003). Rhodope–Pontide Fragment (RPF) is an EW-trending block (Fig. 1A), which is generally divided into a northern zone and a southern zone based on the differences between the rock associations (Akin, 1979; Okay and Şahintürk, 1997; Okay et al., 1997). The initiation of arc magmatism (Upper Cretaceous–Late Paleocene) is related to a northward subduction of the northern branch of Neotethys in the Eastern Pontides (e.g. Akin, 1979; Şengör and Yilmaz, 1981; Okay and Şahintürk, 1997; Yilmaz et al., 1997; Şengör et al., 2003) and the subsequent collision between the Pontides and the Tauride–Anatolide platforms, although the timing of the collision is still controversial (e.g. Robinson et al., 1995; Okay and Şahintürk, 1997; Şen et al., 1998; Şengör et al., 2003). Okay et al. (1997) suggested that the collision should date back to Late Paleocene to Early Eocene, based on field relationships and ages of granitoids. The basement of RPF consists of Devonian metamorphic rocks, Lower Carboniferous granitic and dacitic rocks, Upper Carboniferous–Lower Permian shallow-marine to terrigeneous sedimentary rocks and Permo-Triassic metabasalt–phyllite–marble (e.g. Yilmaz, 1972; Şengör and Yilmaz, 1981; Okay and Şahintürk, 1997; Yilmaz et al., 1997). The basement is overlain by Lower and Middle Jurassic tuffs, pyroclastic and interbedded clastic sedimentary rocks, and Upper Jurassic–Lower Cretaceous carbonates (Şengör and Yilmaz, 1981; Okay and Şahintürk, 1997). Late Mesozoic and Early Cenozoic times are recorded by ophiolitic melange, volcanic and granitoid plutons (e.g. Tokel, 1977; Yilmaz and Boztuğ, 1996; Boztuğ et al., 2004) and these are covered by Upper Paleocene–Lower Eocene major foreland flysch and Post Eocene terrigeneous units (e.g. Okay and Şahintürk, 1997).

The RPF extends for 450 km along the northeastern coast of Turkey (Fig. 1B) and consists of a series of granitoid bodies, which are parts of the composite Kaçkar Batholith, emplaced during Late Cretaceous to Late Eocene times. The granitoid bodies occurred in various geodynamic settings and have different ages (Taner, 1977; Moore et al., 1980) and compositions (Yilmaz and

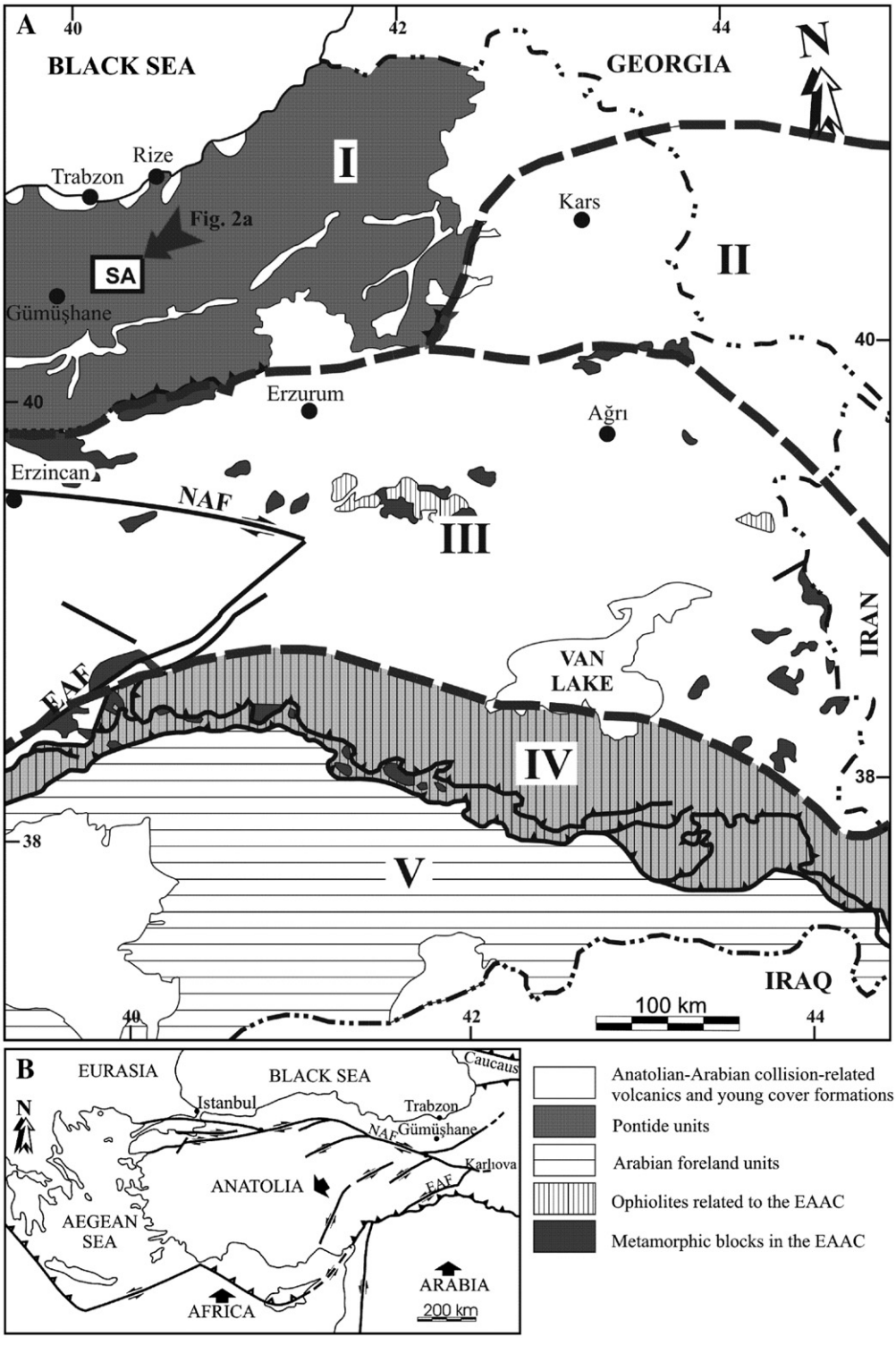

Fig. 1. Simplified geological map displaying major blocks of Eastern Turkey. [Modified after Şengör et al. (2003) and Keskin (2005)]. I: Rhodope–Pontide fragment (RPF), II: Northwest Iranian fragment, III: Eastern Anatolian Accretionary Complex (EAAC), IV: Bitlis-Pötürge Massif, V: Arabian foreland, NAF: North Anatolian fault, EAF: East Anatolian fault, SA: Study area.

Boztuğ, 1996; Karsli et al., 2002; Topuz et al., 2005; Boztuğ et al., 2006; Dokuz et al., 2006). The compositions of the plutons in the RPF vary from low-K tholeiitic through calc-alkaline (rarely high-K) metaluminous granitoids and peraluminous leucogranites to alkaline syenites and monzonites (e.g. Karsli et al., 2002; aahin et al., 2004; Boztuğ et al., 2006). The emplacements took place during the processes of crustal thickening related to the arc-continent collision and subsequent post-collisional extensional regimes (e.g. Yilmaz and Boztuğ, 1996; Karsli et al., 2004a,b; Topuz et al., 2005).

The Dölek and Sariçiçek plutons are part of the composite Kaçkar Batholith, dated 30 to 80 Ma (K–Ar on hornblende; Taner, 1977; Moore et al., 1980). The batholith lies along an E–W trend in the RPF of Eastern Turkey. The Dölek and Sariçiçek plutons are located in the southern part of the RPF (Fig. 2A) and have a wide contact aureole in Early Eocene andesitic rocks of the Alibaba Formation (Fig. 2B). The plutons were dated at 42–44 Ma using K–Ar method on biotite separates in this study.

3. Sample and analytical techniques

Fifty-four samples were taken from the plutons for geochemical analyses [major, trace and rare earth elements (RRE)]. The sampling localities are shown in Fig. 2B. After a petrographic examination to guarantee freshness, rock samples were crushed in specially designed steel jaw crushers and then powdered in an agate mill to a grain size of <200 mesh. Powder aliquots for bulk-rock analyses were prepared by quarter reduction of split from the samples weighting 1–2 kg. Major, trace and rare earth element compositions were determined by commercially operating ACME Laboratories Ltd., Vancouver, Canada. Major elements were measured using an ICP atomic emission spectrometer after fusion with $LiBO_2$, with detection limits around 0.001–0.04%. Trace elements and REEs were determined by the use of ICP mass spectrometer after acid decomposition (HNO_3 of % 5), with detection limits ranging from 0.01 to 0.5 ppm. STD SO-17 was certified in-house against 38 Certified Reference materials including CANMET SY-4 and USGS AGV-1, G-2, GSP-2 and W-2. The analyses are considered accurate within limits of 2–5% for major elements, 10–15% or better for trace elements and 1–5% for REEs.

Rb–Sr, Sm–Nd and Pb isotopic analyses were performed at the Institute of Geology and Geophysics (IGG, Beijing). Samples were dissolved using acid (HF+ $HClO_4$) in sealed Savillex beakers on a hot plate for a week. Separation of Rb, Sr and LREE was done using a cation-exchange column (packed with Bio-Rad AG50Wx8 resin). Sm and Nd were further purified using a second cation-exchange column and then conditioned and eluded with dilute HCI. Mass analyses were performed with a multi-collector VG354 mass spectrometer. Rb, Sr, Sm and Nd concentrations were measured using the isotopic dilution method. $^{87}Sr/^{86}Sr$ ratios were normalized against $^{86}Sr/^{88}Sr=0.1194$. $^{143}Nd/^{144}Nd$ ratios were normalized against $^{146}Nd/^{144}Nd=0.7219$. $^{87}Sr/^{86}Sr$ ratios were adjusted to NBS-987 Sr standart=0.710250 and $^{143}Nd/^{144}Nd$ ratios to La Jolla Nd standart=0.511860. Uncertainties due to the concentration analyses by isotopic dilution is ±2% for Rb, ±0.4–1% for Sr and less than ±0.5% for Sm and Nd depending upon the concentration levels. The overall uncertainty for Rb/Sr is ±2% and ±0.2–0.5% for Sm/Nd. Procedural blanks are: Rb= 120 pg, Sr=200 pg and Nd=50–100 pg. For the analysis of Pb isotope the sample powder was spiked and dissolved in concentrated HF at 800 °C for 72 h. Lead was separated and purified by a conventional anion-exchange technique (AG1x8, 200–400 resin) with diluted HBr. Isotopic ratios were measured using a VG-354 mass spectrometer at the IGG (Beijing). Repeated analyses of NBS981 resulted in $^{204}Pb/^{206}Pb=0.05897\pm15$, $^{207}Pb/^{206}Pb=0.91445\pm80$ and $^{208}Pb/^{206}Pb=2.16170\pm200$.

Mineral compositions were determined using a CAMECA-SX-51 electron microprobe equipped with 5 wavelength-dispersive spectrometers at the Mineralogical Institute of Heidelberg University, Germany. Synthetic and natural oxides and silicates were used for calibration. The correction procedures were based on the CAMECA's PAP algorithm by Pouchou and Pichoir (1985). Detection limits were generally on the order of 0.1 wt.%. The operating conditions were set as 15 kV accelerating voltage and 20 nA beam current. The counting time was usually set to 10 s for the major elements (i.e. Si, Al, Fe, Ca, Na and K). The analyses were performed using a beam of diameter 1 μm except for feldspars, which used a defocused beam (10 μm) in order to minimize the alkaline diffusion.

The K–Ar dating was also performed at the Mineralogical Institute of Heidelberg University, Germany. Biotite separates were obtained by the conventional techniques of cracking, sieving, magnetic and heavy liquid separation, handpicking, and ultrasonic cleaning. The Potassium content was determined by emission flame photometry. The samples (c. 50 mg) were wrapped in Al. ^{38}Ar spike was calibrated using the inter laboratory biotite standard HD-B1 (24.21±0.32 Ma, K 7.956±0.051, $^{40}Ar^*$ 7.536±0.104 nl/g). The argon was extracted by total fusion in an inductive Mo furnace at 1400 °C. To clean the extracted gases Zr–Al getters were used. The Ar isotope

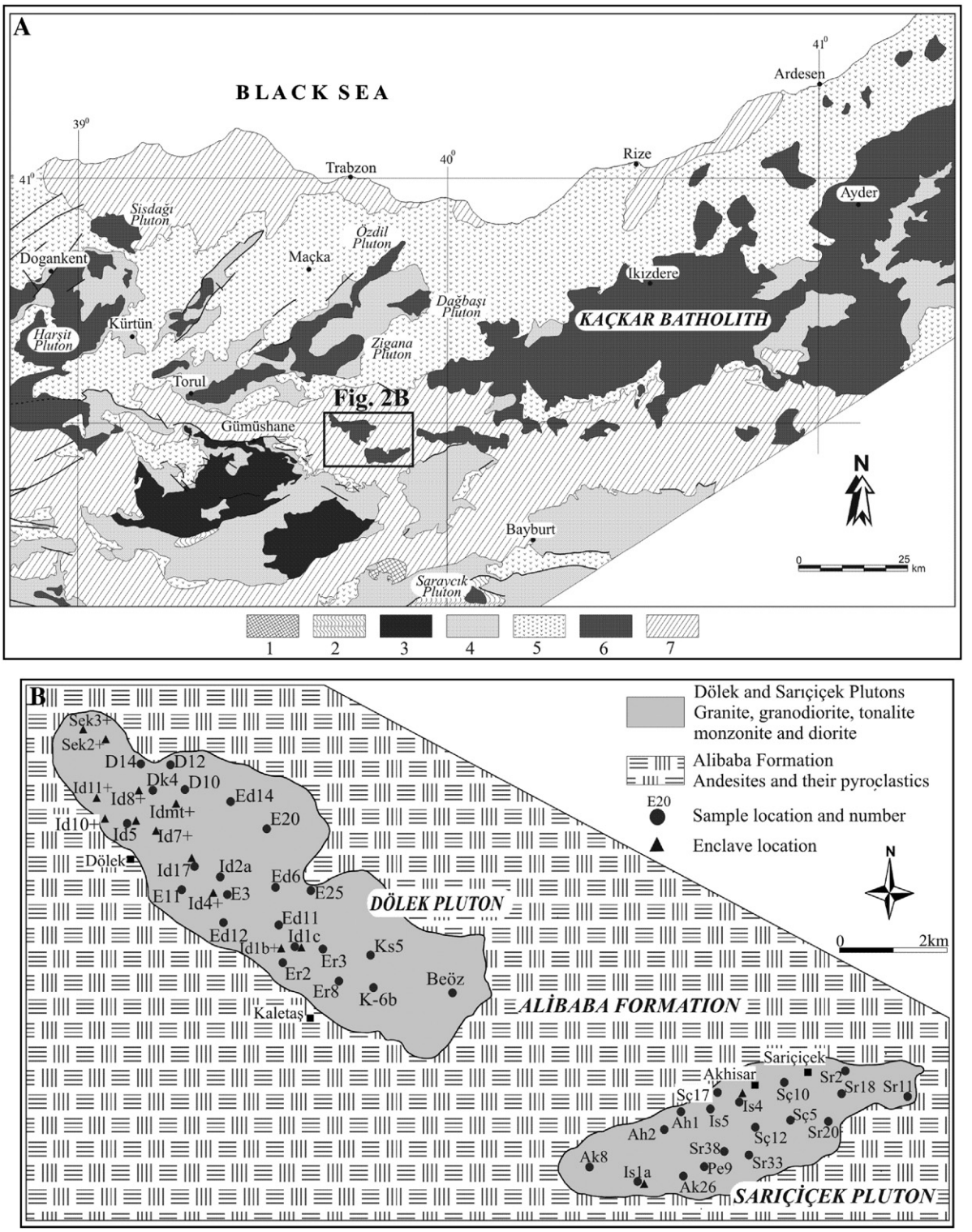

Fig. 2. (A): Simplified geological map of the Pontide units; 1, Permo-Carboniferous terrigeneous; 2, Paleozoic metamorphic rocks; 3, Paleozoic granitoids; 4, Jurassic–Lower Cretaceous units; 5, Upper Cretaceous units; 6, Upper Cretaceous–Eocene granitoids; 7, Tertiary nits. (B): Geological map of the Dölek and Sariçiçek plutons along with the sample locations.

compositions were measured in static mode with a modified Varian-MAT GD150 mass spectrometer (0.38 T permanent magnet, 180°, 5 cm radius of curvature). All the data were corrected for mass discrimination. Constants used for age calculations are those recommended by Steiger and Jäger (1977). $^{40}Ar/^{40}K$ age uncertainties comprise errors due to the argon-measurement of the ^{38}Ar spike and the K-measurement. All error assignments of isotope ratios and ages given in this paper are 2σ.

4. Results

4.1. Petrography and mineral composition

4.1.1. Host rocks

The Dölek and Sariçiçek plutons form outcrops with length less than 10 km and width maximum 4 km. They are made of a variety of rock types including granite, granodiorite, tonalite, monzonite and diorite, with granodiorite and tonalite dominance (~70% of the mass volume). All the rock units share several common petrographic features and are described together. Monzonite and diorite never exceed 25 vol.%. Granite occupies less than 10% of the volume. All rocks closely follow typical calc-alkaline differentiation trend (Fig. 3). The contact relations between all lithotypes are transitional. Main rocks of the plutons are medium-grained (Fig. 4A, B, C) containing larger acicular amphibole (~15 mm; Fig. 4D) and plagioclase grains that display oscillatory zoning (~10 mm; Fig. 4E), which can be attributed to a magma mixing (e.g. Vernon, 1990; Hibbard, 1991; Waight et al., 2000) in a finer-grained matrix of plagioclase (25–73%), K-feldspar (9–42%), quartz (4–35%), amphibole (1–20%), biotite (0–17%), pyroxene (cpx; 0–10%) and iron–titanium oxides (1–7%) in a descending order of abundance. Mafic constituents are represented by amphibole, biotite and pyroxene with amphibole prevailing over biotite and pyroxene. Dioritic and monzonitic rocks contain amphibole and biotite (amphibole > biotite) with abundances more than granitic, granodioritic and tonalitic rocks. Pyroxene is found only in dioritic rocks. A lath shaped plagioclase is commonly observed. Plagioclase ranges in composition from An_{64} to An_{25}, with Or content rarely exceeding 1 mol% (Table 1). Oscillation controlled by An mol% variation changes from 10 to 150 μm in thickness and has ~15 mol% An variation. Orthoclase ($Or_{96\text{-}74}Ab_{3\text{-}26}An_{1\text{-}0}$) contains finer-grained plagioclase, amphibole and biotite (Fig. 4F). Quartz is anhedral and poikilitic and also includes K-feldspar. Green to brownish green amphiboles are generally calcic and characterized by X_{Mg} [=Mg/(Mg+Fe_{tot})]=0.51–0.82. Biotite forms a large subhedral to euhedral crystals (10–15 mm in length) with inclusions of Fe–Ti oxide and apatite (Fig. 4G) and has variable TiO_2 content (3.36–6.50 wt.%) and

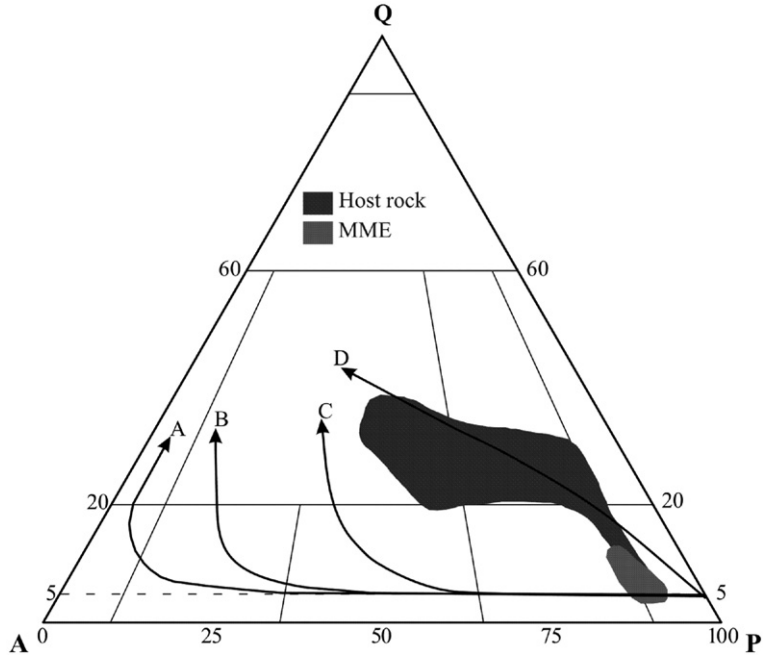

Fig. 3. Modal Q–A–P diagram showing the locations of the representative fields of the Eocene Dölek and Sariçiçek plutons in the field of granite, granodiorite, tonalite, monzonite, diorite and quartz monzodiorite according to the Streckeisen (1976) classification. Arrows show typical differentiation trends (Le Maitre et al., 1989) for magmatic series: Strongly alkaline (A), mildly alkaline (B), monzonitic (C) and calc-alkaline (D).

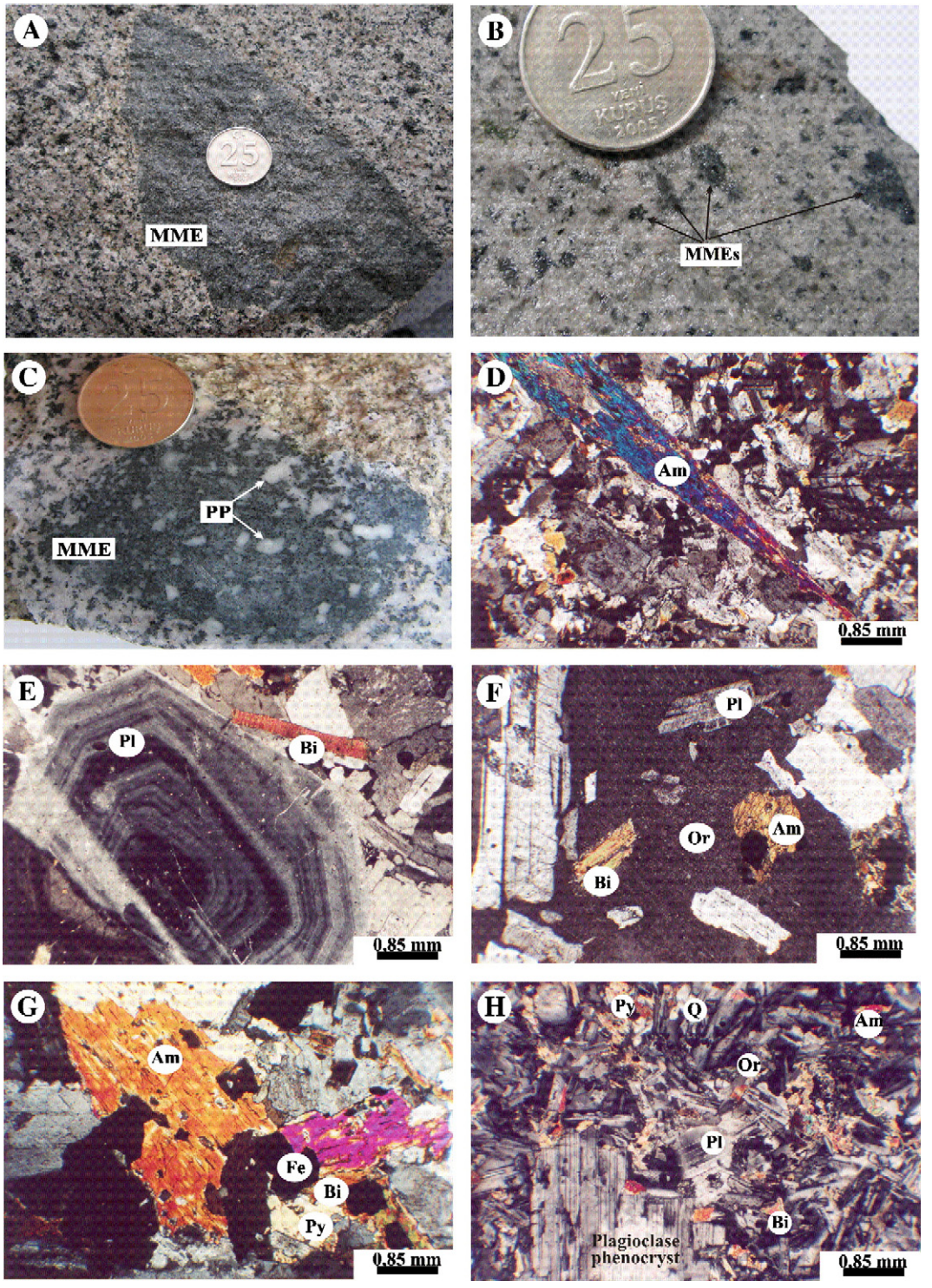

Fig. 4. (A–C) Macroscopic view of mafic microgranular enclaves within the host rocks and (D–H) photomicrograph showing textural relationships of the host granitoid rocks and their enclaves. The features are amphibole (Am), plagioclase (Pl), biotite (Bi), orthoclase (Or), pyroxene (Py), Fe–Ti oxides (Fe) and plagioclase phenocryst (PP).

Table 1
Microprobe analyses (wt.%) of plagioclase in the representative rocks of the Dölek and Sariçiçek plutons

Mineral	Plg	Plg	Plg	Plg	Plg	Plg	Plg	Plg	Plg	Plg	Plg	Plg	Plg	Plg	Plg	Plg	Plg	Plg
Sample	Sr11	D10	Er2	Sr2	Ah2	Ah2	Id2a	Is5	Ed14	E20	Id17+	Id17+	Is4+	Is4+	Is1a+ (p)	Is1a+ (p)	Id1c+	Id1c+
Rock type	gr	gr	grd	grd	tn	tn	mz	mz	dio	dio	gbb.dio	gbb.dio	dio	dio	dio	dio	mz.dio	mz.dio
Area	Rim	Core	Rim	Core	Rim	Core	Rim	Core	Rim	Core	Core	Rim	Core	Rim	Rim	Core	Core	Rim
SiO_2	57.14	52.30	55.88	54.12	61.98	56.88	54.26	53.04	55.37	54.21	55.03	61.58	59.55	62.10	57.73	51.48	53.39	59.31
Al_2O_3	26.31	30.23	27.77	28.85	23.99	26.57	28.33	28.83	27.07	28.83	27.95	24.26	25.64	24.24	26.62	30.73	29.73	25.05
Fe_2O_3	0.23	0.60	0.45	0.46	0.26	0.30	0.35	0.61	0.48	0.34	0.41	0.21	0.37	0.30	0.56	0.57	0.63	0.22
CaO	8.65	12.61	9.93	11.27	5.53	8.33	10.82	12.23	9.83	11.24	10.33	5.29	7.23	5.38	8.35	13.04	11.32	6.40
Na_2O	6.40	4.05	5.69	4.78	8.00	6.58	5.28	4.46	5.78	5.06	5.40	8.25	7.34	8.14	6.57	3.83	4.88	7.99
K_2O	0.29	0.23	0.52	0.26	0.63	0.36	0.31	0.33	0.42	0.16	0.33	0.55	0.33	0.73	0.32	0.25	0.07	0.18
Total	99.02	100.02	100.23	99.74	100.43	99.01	99.35	99.50	99.18	99.85	99.43	100.14	100.45	100.89	100.14	99.91	100.02	99.16
Cations on the basis of 8 oxygens																		
Si	2.586	2.373	2.513	2.451	2.743	2.576	2.466	2.420	2.522	2.453	2.495	2.732	2.648	2.737	2.584	2.343	2.413	2.665
Al	1.403	1.617	1.472	1.540	1.251	1.418	1.517	1.550	1.453	1.537	1.494	1.269	1.344	1.259	1.404	1.648	1.583	1.327
Fe^{3+}	0.008	0.020	0.015	0.016	0.009	0.010	0.012	0.021	0.016	0.012	0.014	0.007	0.012	0.010	0.019	0.020	0.022	0.008
Ca	0.420	0.613	0.478	0.547	0.262	0.404	0.527	0.598	0.480	0.545	0.502	0.251	0.344	0.254	0.400	0.636	0.548	0.308
Na	0.562	0.356	0.496	0.419	0.686	0.578	0.465	0.394	0.511	0.443	0.474	0.710	0.633	0.696	0.570	0.338	0.428	0.696
K	0.017	0.014	0.030	0.015	0.036	0.021	0.018	0.019	0.025	0.009	0.019	0.031	0.018	0.041	0.018	0.015	0.004	0.010
Total	4.996	4.993	5.004	4.988	4.987	5.007	5.005	5.002	5.007	4.999	4.998	5.000	4.999	4.997	4.995	5.000	4.998	5.014
An	42	62	48	55	27	40	52	59	47	55	50	25	34	26	41	63	56	30
Ab	56	36	49	43	70	58	46	39	51	44	48	72	64	71	57	35	43	69
Or	2	2	3	2	3	2	2	2	2	1	2	3	2	3	2	2	1	1

Rock types: gr granite, grd granodiorite, tn tonalite, mz monzonite, dio diorite, mz.dio monzodiorite, gbb.dio gabroic diorite, + mafic microgranular enclave (MME).
(p) phenocryst in mafic microgranular enclaves.

Table 2
Microprobe analyses (wt.%) of amphibole and biotite in the representative rocks of the plutons

Mineral	Am	Am	Am	Am	Am	Am	Am	Am	Am	Bt	Bt	Bt	Bt	Bt	Bt	Bt	Bt	Bt	Bt
Sample	Sr2	Sr33	Ah2	D12	Beöz	E20	Id4+	Is4+	Id1c+	Sr11	Sr33	E25	D12	Id2a	Ed14	Id4+	Id5+	Is4+	Sek2+
Rock type	grd	grd	tn	tn	mz	dio	gbb.dio	dio	mz.dio	gr	grd	tn	tn	mz	dio	gbb.dio	gbb.dio	dio	mz.dio
SiO_2	51.04	48.63	51.57	52.28	50.98	49.29	51.67	50.83	52.44	38.04	39.09	37.54	36.26	37.83	36.87	36.99	36.65	37.57	36.70
TiO_2	0.91	1.14	0.55	0.36	0.42	0.52	0.36	0.57	0.86	5.05	2.79	4.63	5.81	5.06	5.91	4.63	5.37	4.45	5.58
Al_2O_3	3.64	4.71	3.23	2.16	4.32	4.69	2.89	3.42	3.10	12.66	11.93	13.00	13.16	12.15	13.28	13.03	12.46	12.29	12.63
FeO_{tot}	13.37	18.04	13.33	12.35	12.43	16.77	14.97	15.16	9.43	11.11	13.89	15.68	16.23	14.34	14.14	13.80	15.71	17.73	15.83
MnO	0.54	0.57	0.42	0.52	0.74	0.41	0.46	0.29	0.21	0.18	0.22	0.34	0.34	0.13	0.24	0.24	0.15	0.13	0.20
MgO	15.49	12.52	15.65	16.50	16.36	12.83	13.89	14.73	18.23	17.70	17.68	14.80	13.52	15.64	14.71	17.15	13.95	13.88	13.72
CaO	11.41	10.20	11.23	12.00	10.98	11.93	12.18	11.39	11.59	0.00	0.00	0.00	0.00	0.00	0.00	0.00	0.00	0.00	0.00
Na_2O	1.12	1.69	1.07	0.58	0.97	0.75	0.49	0.86	1.08	0.36	0.18	0.14	0.31	0.20	0.28	0.17	0.23	0.26	0.28
K_2O	0.38	0.52	0.30	0.21	0.35	0.48	0.27	0.38	0.28	8.94	8.35	8.80	8.77	9.54	9.13	7.12	8.98	8.91	8.92
Total	97.89	98.01	97.35	96.93	97.54	97.68	97.18	97.64	97.22	94.02	94.13	94.91	94.39	94.90	94.57	93.12	93.49	95.22	93.85
Cations on the basis of 23 oxygens (amphibole) and 11 oxygens (biotite)																			
Si	7.325	7.106	7.425	7.538	7.295	7.222	7.550	7.366	7.423	2.817	2.919	2.823	2.762	2.828	2.762	2.782	2.811	2.848	2.805
Ti	0.098	0.126	0.059	0.039	0.045	0.058	0.039	0.062	0.091	0.281	0.157	0.262	0.333	0.285	0.333	0.262	0.310	0.253	0.321
Al	0.616	0.811	0.548	0.367	0.728	0.810	0.498	0.584	0.518	1.105	1.050	1.152	1.181	1.071	1.172	1.155	1.126	1.098	1.137
Fe^{3+}	0.779	1.103	0.727	0.596	0.794	0.754	0.412	0.729	0.697	–	–	–	–	–	–	–	–	–	–
Fe^{2+}	0.738	0.979	0.797	0.827	0.606	1.217	1.372	1.027	0.341	0.676	0.890	1.016	1.064	0.881	0.871	0.900	1.034	1.156	1.045
Mn	0.066	0.070	0.052	0.064	0.090	0.051	0.057	0.036	0.025	0.011	0.014	0.021	0.022	0.008	0.015	0.015	0.009	0.009	0.013
Mg	3.313	2.726	3.359	3.546	3.489	2.803	3.026	3.183	3.848	1.954	1.968	1.659	1.535	1.743	1.643	1.922	1.595	1.568	1.563
Ca	1.754	1.596	1.732	1.853	1.684	1.873	1.907	1.768	1.757	0.000	0.000	0.000	0.000	0.000	0.000	0.000	0.000	0.000	0.000
Na	0.311	0.478	0.299	0.163	0.268	0.213	0.139	0.243	0.297	0.052	0.026	0.020	0.045	0.029	0.041	0.025	0.034	0.039	0.041
K	0.069	0.096	0.055	0.038	0.064	0.090	0.051	0.070	0.051	0.845	0.795	0.844	0.852	0.910	0.873	0.683	0.878	0.862	0.869
Total	15.07	15.09	15.05	15.03	15.06	15.09	15.05	15.07	15.05	7.741	7.819	7.797	7.794	7.827	7.710	7.744	7.797	7.833	7.794

Abbreviations as in Table 1.

X_{Mg} of 0.53 to 0.73 (Table 2). Blade biotite was also observed in the host rocks (Fig. 4E). Pyroxene occurs as small, yellowish green subhedral grains (~1 mm) (Fig. 4G). Diopsidic, salitic and augitic pyroxenes have X_{Mg} ranging from 0.66 to 0.78. Fe–Ti oxides coexist with mafic silicates (Fig. 4G). Large titanomagnetite ($Mt_{98\text{-}70}Usp_{30\text{-}02}$) surrounded by finer-grained ilmenite ($Ilm_{99\text{-}65}Hm_{35\text{-}01}$) shows well-developed exsolution lamellae. Apatite exists as irregular blobs within titanomagnetite, biotite, amphibole and plagioclase. Sphene is concentrated around large titanomagnetite, but some of them form as aggregates of twinned crystals. Zircon is an accessory phase in all rock types of the considered plutons and occurs as prismatic crystals (Table 3).

4.1.2. Mafic microgranular enclaves

The MMEs are widespread within the plutons, but their spatial distribution is heterogeneous, mainly concentrated in facies of more felsic. They are mostly elongated in the direction of the long axis of the granitoid bodies. When compared to the host rocks, the MMEs are fine-grained and gabbroic diorite, diorite and quartz monzodiorite in composition. They have ellipsoidal and flattened shapes. These features suggesting plastic behavior at the moment of their incorporation into the hybrid host magma are due to their plastic rheology (Frost and Mahood, 1987; Poli and Tommasini, 1991). The MMEs are commonly 1 mm to 30 cm in size (Fig. 4A, B, C). Larger MMEs never occur in the plutons. The contact with their host is sharp, rounded or irregular, but diffuse contacts without deformation are also observed, which can be attributed to the undercooling and mingling of hybrid MME globules formed by a mixture of mafic and felsic magmas (e.g. Perugini et al., 2004). The degree of thermal, rheological and compositional contrast of co-existing mafic and felsic magmas governs the hybridization levels preserving the megascopic features relevant to the magma mixing (e.g. Kumar et al., 2004). The MMEs show magmatic textures similar to poikilitic–equigranular textures of basic igneous rocks. In addition, no cumulate textures are found in the MMEs. The MMEs contain higher ferromagnesian phases and plagioclase and lower quartz and K-feldspar than those of the host rocks. They are composed of plagioclase (56–76%), amphibole (6–20%), biotite (1–8%), pyroxene (1–7%), orthoclase (3–7%), quartz (2–8%) and Fe–Ti oxides (2–4%) and also contain rounded and large plagioclases, which are compositionally similar to those in the host rocks (Samples Isa+ (p), Sr11 and D10; Table 1) (Fig. 4C, H). In some cases, the large plagioclases crosscut the enclave/host boundary. These features, common in the enclaves worldwide, are considered to prove a liquid state of the enclaves upon their incorporation into the more felsic magma (e.g. Vernon, 1984; Perugini et al., 2003). In addition, the host rock mafic xenocrysts are absent within the MMEs. Titanomagnetite is always present and the rimming titanite is observed less frequently. Small ilmenites and acicular

Table 3
Microprobe analyses (wt.%) of Fe–Ti oxide in the representative rock types of the plutons

Mineral	Fe–Ti	Fe–Ti	Fe–Ti	Fe–Ti	Fe–Ti	Fe–Ti	Fe–Ti	Fe–Ti	Fe–Ti	Fe–Ti	Fe–Ti	Fe–Ti	Fe–Ti	Fe–Ti	Fe–Ti	Fe–Ti	Fe–Ti
Sample	Sr11	Sr11	E11	E11	D12	D12	D12	Id2a	Id2a	Ed12	Ed12	Id17+	Id17+	Is4+	Is4+	Sek2+	Sek2+
Rock type	gr	gr	grd	grd	tn	tn	tn	mz	mz	dio	dio	gbb.dio	gbb.dio	dio	dio	mz.dio	mz.dio
SiO_2	0.04	0.02	0.01	0.23	0.06	0.01	0.32	0.06	0.05	0.20	0.04	0.02	0.00	0.03	0.00	0.05	0.07
TiO_2	3.17	45.55	0.79	48.94	3.70	0.21	47.40	0.62	44.20	0.19	50.07	0.28	50.96	0.46	46.97	1.38	48.59
Al_2O_3	0.15	0.00	0.67	0.05	0.62	0.05	0.00	0.03	0.02	0.00	0.14	0.73	0.00	0.24	0.00	0.91	0.00
$Fe_2O_3^*$	62.85	13.10	66.26	6.40	60.02	69.27	9.89	67.85	17.21	66.75	3.91	67.65	2.92	67.73	11.22	65.27	6.82
FeO	33.72	34.54	31.58	38.50	33.62	31.27	36.69	31.57	34.71	30.90	39.51	31.29	37.89	31.43	35.68	32.31	38.56
MnO	0.40	6.06	0.09	5.16	0.49	0.08	5.01	0.11	4.66	0.00	4.85	0.09	7.07	0.06	6.33	0.19	4.80
MgO	0.02	0.09	0.00	0.31	0.10	0.00	0.06	0.00	0.13	0.06	0.28	0.01	0.26	0.00	0.05	0.05	0.14
Total	100.35	99.36	99.40	99.60	98.61	100.84	100.37	100.23	100.97	98.39	98.83	100.06	99.09	99.95	100.25	100.15	98.99
Cations on the basis of 4 oxygens (magnetite) and 3 oxygens (ilmenite)																	
Si	0.002	0.001	0.000	0.006	0.002	0.000	0.008	0.002	0.001	0.008	0.001	0.001	0.000	0.001	0.000	0.002	0.002
Ti	0.091	0.873	0.023	0.932	0.108	0.006	0.898	0.018	0.836	0.006	0.960	0.008	0.972	0.013	0.893	0.040	0.932
Al	0.007	0.000	0.030	0.001	0.028	0.002	0.000	0.010	0.001	0.013	0.004	0.033	0.000	0.011	0.000	0.041	0.000
Fe^{3+}	1.805	0.251	1.921	0.122	1.748	1.984	0.187	1.955	0.326	1.958	0.075	1.949	0.056	1.955	0.214	1.873	0.131
Fe^{2+}	1.077	0.736	1.017	0.816	1.088	0.996	0.773	1.011	0.730	1.008	0.842	1.002	0.804	1.008	0.755	1.031	0.823
Mn	0.013	0.131	0.003	0.111	0.016	0.002	0.107	0.003	0.099	0.000	0.105	0.003	0.152	0.002	0.136	0.006	0.104
Mg	0.001	0.003	0.000	0.012	0.006	0.000	0.002	0.000	0.005	0.003	0.011	0.001	0.010	0.000	0.002	0.003	0.005
Total	2.996	1.995	2.994	2.000	2.996	2.990	1.975	2.999	1.998	2.996	1.998	2.997	1.994	2.990	2.000	2.996	1.997

Abbreviations as in Table 1. Fe_2O_3 and FeO concentrations are calculated assuming spinel stoichiometry.

Table 4
Temperature (°C), pressure (kbar) and log fO_2 (bar) ranges estimated for the plutons

Sample	Pairs		Estimated temperature (°C) (Blundy and Holland, 1990)	Estimated pressure (kbar) (Schmidt, 1992)	Estimated temperature (°C) (Spencer and Lindsley, 1981)	log fO_2 (bar) (Spencer and Lindsley, 1981)
	Al pfu−Pl Ab	$a_{ulvo}-a_{ilm}$				
Granite[h]	0.91–60	0.29–0.026	653	1.3	617	−20.50
Granodiorite[h]	1.00–54	0.30–0.053	682	1.8	687	−17.65
Tonalite[h]	1.24–44	0.34–0.049	725	2.8	700	−17.50
Monzonite[h]	0.95–57	0.29–0.038	677	1.5	650	−19.30
Diorite[h]	1.44–40	0.40–0.068	768	3.8	757	−15.30
Diorite[h]	1.12–45	0.29–0.058	715	2.3	702	−16.80
Diorite[h]	1.34–43	0.29–0.062	740	3.4	715	−16.25
Gabroicdiorite[e]	1.29–41	0.30–0.077	753	3.1	735	−15.39
Diorite[e]	0.99–53	0.30–0.041	681	1.7	669	−18.96
Diorite[e]	0.90–59	0.29–0.034	664	1.3	645	−19.81
Monzodiorite[e]	0.83–56	0.29–0.030	660	1.0	622	−20.80
Monzodiorite[e]	1.12–47	0.28–0.051	710	2.3	686	−17.75

Al pfu Aluminum per formula.
Pl Ab Albite content in plagioclase.
h host rock; e mafic microgranular enclave.

apatites also occur as accessories. The presence of acicular apatite and quartz ocelli reflects on the hybridization process associated with the generation of the MMEs. The mineral assemblage and mineral compositions of mafic enclaves are similar to those in the host rocks.

4.2. P–T conditions and emplacement depth

Thermobarometric formulations were developed from empirical and theoretical analysis of the calc-alkaline plutons and were experimentally calibrated assuming a mineral assemblage made of amphibole, biotite, plagioclase, quartz, alkali feldspar, spinel, magnetite or ilmenite near H_2O-saturated solidus and oxygen fugacities (fO_2) bracketed between the nickel–nickel oxide (NNO) and hematite–magnetite (HM) buffers. The plutons under consideration have the appropriate mineralogy required for the application of hornblende–plagioclase thermometer (Blundy and Holland, 1990) and Al-in hornblende barometer (Schmidt, 1992). The contact relationships between the phases are also important in thermobarometry. Therefore, great care was taken to measure the rims of the crystals in equilibrium to estimate the approximate *P–T* values. Although the amphibole cores and the rims show no significant difference in the Al content, we used the rim composition of the amphibole in contact with the interstitial quartz and/or orthoclase representing a late-stage (near-solidus) crystallization of the magma. The results are listed in Table 4. Accordingly, the pressures obtained from the host rocks and also their enclaves have the ranges 1.3±0.1 to 3.8±0.7 and 1.0±0.1 to 3.1±0.6 kbar, respectively, which correspond to the emplacement depth of ~5–9 km. The temperatures are estimated to have the ranges 623±7–768±23 °C and 620±7–753±22 °C, respectively. These temperature estimates are consistent with those of the Fe–Ti oxide thermobarometer by Spencer and Lindsley (1981), which requires coexistence of ilmenite and titanomagnetite. The estimated temperatures are in the range of 655–755 °C (host rocks) and 685–782 °C (MMEs). The wide range (1.3 to 3.8 kbar) of pressure condition of crystallization may suggest an extensional or transitional condition in the crust and/or may also be caused by some subsolidus transformation to actinolitic amphibole, which is present in some

Table 5
K–Ar isotope data on the biotite separates from the Dölek and Sarıçiçek plutons

Sample	Rock type	Pluton	Mineral	Weight [mgr]	K [%][a] (±1 Φ)	$^{40}Ar^*$ [nl/g] (±1 Φ)	$^{40}Ar^*$ [%]	t[Ma] (±1 Φ)[b]
Id2a	mz	Dölek	bt	70.33	7.80±0.08	13.26±0.23	84.4	42.9±1.81
D10	gr	Dölek	bt	72.50	6.70±0.07	11.47±0.21	84.2	43.5±1.82
Ah2	tn	Sarıçiçek	bt	68.62	7.00±0.07	12.15±0.28	80.2	44.1±2.22
Is5	mz	Sarıçiçek	bt	70.40	5.15±0.05	8.64±0.44	64.4	42.7±2.21

[a] Determined by emission flame photometry.
[b] Constants used for age calculations are those recommended by Steiger and Jäger (1977).

Table 6
Whole-rock chemical analyses for the rocks from the Dölek and Sariçiçek plutons

Sample	Sr11	D10	Id1c	Sç12	Sr2	Sr33	Ks5	E11	Er2	Er3	E3	E25	D12	K-6b	Pe9	Er8	Sç5	Sç10	Sç17	Is1a
Rock type	gr	gr	grd	grd	grd	grd	grd	grd	grd	grd	tn	tn	tn	tn	tn	tn	tn	tn	tn	tn
SiO_2	72.67	70.12	69.04	65.16	65.33	65.66	68.31	65.83	67.92	68.17	61.31	61.93	64.60	61.50	62.07	64.51	64.29	64.57	63.41	62.92
TiO_2	0.35	0.38	0.49	0.65	0.65	0.63	0.44	0.53	0.55	0.49	0.65	0.65	0.52	0.70	0.71	0.60	0.64	0.63	0.68	0.69
Al_2O_3	14.03	14.50	15.30	15.48	15.67	15.70	14.88	15.84	16.25	15.26	16.02	15.47	15.71	15.97	15.45	16.15	15.34	15.75	15.93	15.58
$Fe_2O_3^t$	2.65	3.04	2.23	5.41	5.24	4.98	3.53	4.86	2.72	2.50	6.11	6.10	4.94	6.45	6.25	4.91	5.38	5.27	5.72	5.70
MnO	0.04	0.05	0.02	0.10	0.09	0.10	0.06	0.11	0.03	0.02	0.11	0.11	0.09	0.13	0.10	0.06	0.10	0.10	0.11	0.11
MgO	0.78	1.22	0.84	2.14	2.23	1.93	1.25	1.68	1.10	0.93	2.52	2.51	2.10	2.87	2.48	1.99	2.15	2.20	2.49	2.20
CaO	1.72	1.98	3.03	4.17	3.90	4.37	3.38	3.99	3.64	3.22	5.36	5.11	4.17	5.49	5.19	4.65	4.39	4.54	4.65	4.59
Na_2O	2.98	3.02	3.95	3.33	3.29	3.07	3.17	3.19	5.86	4.09	3.18	3.21	2.86	3.02	3.27	3.78	3.13	3.36	3.31	3.93
K_2O	4.43	5.08	4.17	3.56	3.47	3.42	4.19	3.50	1.31	3.78	3.23	3.36	4.13	2.95	3.06	2.89	3.26	3.27	3.19	3.00
P_2O_5	0.06	0.08	0.12	0.12	0.12	0.12	0.09	0.13	0.13	0.10	0.14	0.14	0.12	0.15	0.15	0.15	0.14	0.15	0.15	0.16
LOI	1.12	0.94	0.40	0.81	0.73	1.00	0.30	0.83	0.82	1.50	1.35	0.64	0.94	0.92	0.37	0.41	0.88	1.11	1.16	1.53
Total	100.82	100.41	99.59	100.92	100.73	100.96	99.59	100.51	100.32	100.05	99.99	99.22	100.18	100.14	99.10	100.10	99.70	100.95	100.80	100.41
Mg#	36.8	44.3	42.7	43.9	45.7	43.4	41.2	40.6	44.5	42.4	45.0	45.0	45.7	46.8	44.0	44.5	44.2	45.3	46.3	43.3
ASI	1.09	1.03	0.93	0.92	0.96	0.94	0.94	0.97	0.92	0.92	0.87	0.85	0.94	0.88	0.85	0.91	0.92	0.91	0.92	0.86
Rb	144	173	70	106	110	116	139	101	19	57	92	102	141	81	95	70	101	100	95	103
Sr	206	213	300	290	277	320	230	353	358	305	342	233	321	350	303	327	285	313	318	288
Ba	1,095	650	809	846	817	740	653	860	574	985	727	704	679	664	653	775	705	629	723	513
Cs	6.90	–	–	–	–	–	–	–	–	–	–	–	5.10	–	2.70	0.60	–	–	3.20	1.93
Zr	202	186	227	252	209	187	192	178	210	207	175	184	185	180	180	154	178	221	204	234
Hf	5.80	–	–	–	–	–	–	–	–	–	–	–	5.60	–	5.30	4.80	–	–	5.50	5.83
Th	15	10	9	10	11	12	11	12	9	10	11	11	17	9	10	7	3	11	9	10
Pb	30	22	9	34	25	43	32	47	6	6	17	30	19	46	27	8	51	19	25	22
Nb	10	13	8	10	10	10	10	9	11	11	9	9	10	9	10	8	10	8	9	9
Y	25	28	25	26	30	25	27	25	28	26	26	28	26	29	28	30	27	30	26	31
Cr	18	11	13	14	14	8	14	13	5	16	10	16	16	21	18	18	17	13	14	15
Ni	5	5	5	7	7	6	5	6	5	5	7	8	8	10	8	6	7	7	8	8
Co	n.a.	10	5	11	11	12	14	20	20	2	12	14	7	17	11	20	11	11	13	12
V	34	83	52	107	96	94	58	102	65	47	123	126	99	132	121	106	102	74	115	92
Zn	30	23	10	48	46	48	40	70	9	9	52	60	45	78	57	14	62	42	56	53
La	29.70	–	–	–	–	–	–	–	–	–	–	–	25.90	–	33.50	26.90	–	–	27.80	32.00
Ce	60.10	–	–	–	–	–	–	–	–	–	–	–	53.60	–	66.40	53.30	–	–	56.10	64.20
Pr	6.20	–	–	–	–	–	–	–	–	–	–	–	5.98	–	750	5.89	–	–	6.21	7.34
Nd	22.10	–	–	–	–	–	–	–	–	–	–	–	21.80	–	28.10	22.10	–	–	24.30	27.50
Sm	4.50	–	–	–	–	–	–	–	–	–	–	–	4.70	–	6.50	4.50	–	–	4.79	5.49
Eu	0.82	–	–	–	–	–	–	–	–	–	–	–	0.99	–	1.23	0.82	–	–	1.00	1.06
Gd	3.69	–	–	–	–	–	–	–	–	–	–	–	4.06	–	5.21	3.69	–	–	4.42	5.03
Tb	0.60	–	–	–	–	–	–	–	–	–	–	–	0.66	–	0.80	0.60	–	–	0.70	0.77
Dy	3.83	–	–	–	–	–	–	–	–	–	–	–	4.14	–	5.21	3.83	–	–	4.30	4.78
Ho	0.77	–	–	–	–	–	–	–	–	–	–	–	0.86	–	1.04	0.77	–	–	0.88	0.98
Er	2.44	–	–	–	–	–	–	–	–	–	–	–	2.78	–	3.25	2.44	–	–	3.00	2.93
Tm	0.34	–	–	–	–	–	–	–	–	–	–	–	0.35	–	0.44	0.34	–	–	0.39	0.42
Yb	2.36	–	–	–	–	–	–	–	–	–	–	–	2.58	–	2.93	2.36	–	–	2.69	2.91
Lu	0.39	–	–	–	–	–	–	–	–	–	–	–	0.44	–	0.46	0.39	–	–	0.38	0.44
(Gd/Yb)cn	1.26												1.27		1.43	1.26			1.33	1.39
(La/Yb)cn	8.48	–	–	–	–	–	–	–		–	–	–	6.77	–	7.71	8.48	–	–	6.97	7.41
Eu/Eu*	0.62	–	–	–	–	–	–	–	–	–	–	–	0.69	–	0.63	0.62	–	–	0.64	0.62

Sample	Is4	Sr18	Sr20	Sr38	Ah1	Ah2	Ak8	Ak26	Dk4	Is5	Id17	Ed14	Id2a	Id5	Beöz	D14	Ed6	Ed11	Ed12	E20
Rock type	tn	tn	tn	tn	tn	tn	tn	tn	tn	tn	tn	tn	mz	mz	mz	dio	dio	dio	dio	dio
SiO_2	62.49	64.68	64.42	63.68	61.83	62.60	63.67	62.93	63.12	60.83	61.85	60.50	59.83	60.51	59.43	57.74	57.35	57.85	56.98	57.11
TiO_2	0.68	0.64	0.66	0.70	0.65	0.74	0.64	0.72	0.56	0.73	0.68	0.66	0.76	0.66	0.70	0.75	0.66	0.79	0.82	0.82
Al_2O_3	15.82	15.52	15.65	15.16	16.02	15.49	15.18	15.28	15.63	16.04	16.15	16.18	15.75	16.58	16.92	16.82	16.72	16.61	17.22	16.60
$Fe_2O_3^t$	5.97	5.20	5.51	5.46	5.88	5.91	5.41	5.79	5.20	6.31	6.12	6.36	6.39	6.30	6.34	7.27	7.49	7.97	8.17	8.04
MnO	0.11	0.10	0.10	0.11	0.11	0.10	0.09	0.12	0.09	0.12	0.11	0.12	0.16	0.10	0.13	0.11	0.14	0.13	0.18	0.15
MgO	2.47	2.30	2.20	2.38	2.35	2.47	2.14	2.20	2.14	2.82	2.38	3.02	2.92	2.80	2.68	3.64	3.78	3.60	3.79	3.70
CaO	5.10	4.28	4.51	4.04	5.09	4.43	3.90	4.27	4.35	5.40	5.17	5.08	5.15	5.45	6.03	5.83	6.43	6.51	6.77	6.67
Na_2O	3.22	3.29	3.43	3.52	3.27	3.35	3.61	3.55	3.09	3.55	3.44	3.16	2.99	3.20	3.46	3.26	3.04	3.00	3.08	3.21
K_2O	3.09	3.36	3.23	3.46	2.94	3.01	3.52	3.57	4.16	2.72	3.15	3.50	4.02	3.30	3.03	2.93	2.15	2.16	2.31	2.63
P_2O_5	0.16	0.15	0.12	0.11	0.14	0.12	0.13	0.14	0.13	0.14	0.15	0.14	0.14	0.19	0.16	0.15	0.15	0.16	0.19	0.17
LOI	0.86	0.85	0.92	1.10	0.87	1.60	0.85	0.71	0.60	1.10	1.04	1.10	1.70	0.84	0.90	1.30	1.12	1.33	1.54	0.70
Total	99.97	100.37	100.74	99.82	99.14	99.98	99.13	99.28	99.07	99.76	100.24	100.01	99.97	99.93	100.36	99.80	99.03	100.11	101.05	99.80
Mg#	45.0	46.7	44.2	46.3	44.2	43.9	43.9	42.9	44.9	47.0	43.5	47.2	47.5	46.8	45.6	49.8	50.0	47.2	47.9	47.7
ASI	0.88	0.92	0.90	0.90	0.90	0.93	0.90	0.88	0.89	0.86	0.87	0.90	0.85	0.89	0.85	0.88	0.88	0.87	0.87	0.82
Rb	93	103	96	96	87	100	106	111	133	90	86	111	129	98	87	107	49	49	55	86
Sr	315	276	310	268	344	283	291	294	320	372	390	364	351	401	494	450	466	410	424	417
Ba	644	610	713	835	702	671	805	778	718	714	670	660	790	672	979	802	767	532	580	573
Cs	2.55	–	–	3.20	–	2.80	–	–	–	2.6	1.06	2.3	4.50	2.26	1.4	2.40	0.70	0.60	0.80	4.30
Zr	175	227	196	158	233	208	406	196	192	177	237	190	98	180	122	198	137	135	185	153
Hf	3.14	–	–	5.10	–	6.10	–	–	–	5.1	3.76	5.2	4.00	2.43	3.9	4.90	3.80	3.60	4.20	4.60
Th	9	11	10	10	10	9	12	10	16	11	9	12	12	11	9	12	8	7	6	10
Nb	9	8	10	9	8	7	10	11	10	9	8	10	10	9	8	8	6	7	8	8
Pb	46	17	18	n.a	17	19	56	23	21	n.a	21	21	n.a.	25	n.a.	n.a.	9	14	25	68
Y	26	30	26	26	26	28	30	31	23	28	24	29	23	24	22	24	24	21	24	27
Cr	18	14	15	n.a.	14	20	19	16	10	n.a.	16	22	n.a.	16	n.a.	n.a.	14	18	22	24
Ni	9	7	7	9	7	8	6	7	8	29	10	9	30	10	10	17	13	11	11	9
Co	14	14	12	12	15	11	20	20	20	17	16	10	16	15	14	21	20	22	20	17
V	98	58	121	93	129	90	111	127	109	133	95	104	134	109	122	172	179	181	158	186
Zn	79	41	41	n.a.	51	45	53	60	36	n.a.	38	43	n.a.	38	n.a.	n.a.	46	49	69	100
La	27.20	–	–	26.30	–	30.20	–	–	–	28.80	25.50	27.70	26.30	26.50	24.40	28.40	19.70	26.50	17.60	27.40
Ce	55.00	–	–	54.20	–	60.80	–	–	–	58.70	49.60	57.10	54.20	51.70	47.60	56.30	38.70	53.30	37.50	56.90
Pr	6.37	–	–	6.15	–	6.94	–	–	–	6.67	5.56	6.49	6.05	5.94	5.15	6.50	4.37	5.82	4.46	6.36
Nd	24.30	–	–	23.10	–	26.90	–	–	–	25.30	21.00	24.50	22.70	22.40	20.30	25.60	18.10	22.30	18.40	25.10
Sm	5.00	–	–	4.80	–	5.50	–	–	–	5.30	4.23	5.50	4.60	4.63	4.01	5.10	3.90	4.90	4.50	5.30
Eu	1.09	–	–	1.06	–	1.24	–	–	–	1.20	1.07	1.24	1.01	1.03	1.15	1.35	0.92	1.17	1.09	1.27
Gd	4.55	–	–	4.54	–	5.08	–	–	–	5.02	4.00	4.84	4.23	4.13	4.02	4.64	3.73	4.11	3.98	4.74
Tb	0.70	–	–	0.74	–	0.83	–	–	–	0.77	0.60	0.76	0.68	0.64	0.61	0.68	0.57	0.65	0.68	0.77
Dy	4.37	–	–	4.34	–	5.05	–	–	–	4.94	3.84	4.85	4.44	3.94	3.95	4.38	4.00	3.69	4.09	4.82
Ho	0.88	–	–	0.90	–	0.99	–	–	–	1.01	0.78	0.94	0.88	0.79	0.78	1.00	0.74	0.76	0.82	0.95
Er	2.60	–	–	2.85	–	3.05	–	–	–	3.19	2.36	3.08	2.77	2.40	2.52	2.84	2.49	2.38	2.68	3.06
Tm	0.38	–	–	0.38	–	0.44	–	–	–	0.40	0.34	0.40	0.36	0.35	0.33	0.37	0.33	0.32	0.36	0.40
Yb	2.46	–	–	2.56	–	2.82	–	–	–	2.85	2.29	2.80	2.47	2.31	2.27	2.84	2.20	2.10	2.32	2.85
Lu	0.37	–	–	0.38	–	0.45	–	–	–	0.42	0.35	0.48	0.39	0.35	0.39	0.42	0.34	0.31	0.35	0.45
(Gd/Yb)cn	1.49			1.43		1.45				1.42	1.41	1.39	1.38	1.44	1.43	1.32	1.37	1.58	1.38	1.34
(La/Yb)cn	7.45	–	–	6.93	–	7.22	–	–	–	6.81	7.51	6.67	7.18	7.73	7.25	6.74	6.04	8.51	5.11	6.48
Eu/Eu*	0.69	–	–	0.69	–	0.70	–	–	–	0.71	0.78	0.73	0.69	0.72	0.88	0.83	0.72	0.78	0.77	0.62

(continued on next page)

Table 6 (*continued*)

Sample	Id4+	Id1b+	Sek3+	Idmt+	Id10+	Is4+	Is1a+	Id5+	Id11+	Id17+	Id7+	Sek2+	Id8+	Id1c+
Rock type	gbb.dio	gbb.dio	gbb.dio	gbb.dio	gbb.dio	dio	dio	mz.dio	mz.dio	mz.dio	mz.dio	mz.dio	mz.dio	mz.dio
SiO_2	54.64	56.46	54.85	55.61	56.35	57.38	60.94	54.36	53.21	53.90	55.28	54.56	54.66	55.94
TiO_2	0.82	0.77	0.75	0.85	0.73	0.80	0.70	0.92	0.79	0.94	0.89	0.81	0.82	0.79
Al_2O_3	17.10	17.01	17.98	17.33	16.60	16.93	16.25	18.01	17.10	16.80	17.40	17.66	17.44	17.93
$Fe_2O_3^{tot}$	8.80	8.66	8.73	8.40	8.50	7.90	6.66	8.97	8.66	9.11	8.78	8.90	8.22	7.99
MnO	0.18	0.15	0.17	0.20	0.19	0.15	0.11	0.16	0.18	0.16	0.17	0.19	0.19	0.07
MgO	4.35	3.94	4.70	4.02	4.16	3.85	2.77	3.68	5.03	4.46	4.15	4.05	4.57	3.59
CaO	8.66	7.35	7.56	7.76	6.84	7.52	5.47	7.58	7.83	7.51	7.15	7.68	6.89	7.60
Na_2O	3.22	3.80	3.25	3.56	3.61	3.15	3.87	4.53	3.36	3.87	3.79	3.36	3.37	4.28
K_2O	1.62	1.39	1.78	1.96	2.06	1.55	2.32	1.09	1.97	1.73	1.81	2.37	2.59	1.51
P_2O_5	0.16	0.14	0.16	0.20	0.18	0.16	0.17	0.16	0.12	0.16	0.22	0.19	0.15	0.18
LOI	1.56	0.98	1.17	0.89	1.15	0.85	1.50	0.72	0.78	0.92	1.14	0.31	0.83	0.83
Total	101.11	100.65	101.10	100.78	100.37	100.24	100.76	100.18	99.03	99.56	100.78	100.04	99.73	100.71
Mg#	49.5	47.4	51.6	48.7	49.2	49.1	45.2	44.4	53.5	49.2	48.4	47.4	52.4	47.1
ASI	0.75	0.81	0.86	0.79	0.81	0.83	0.86	0.80	0.78	0.77	0.82	0.80	0.84	0.80
Rb	57	49	72	77	85	54	77	35	72	50	67	89	88	34
Sr	375	372	433	420	358	380	324	454	421	441	415	383	410	454
Ba	442	407	384	403	470	493	525	207	399	420	379	365	476	350
Cs	1.17	1.49	2.90	2.76	2.85	1.78	1.99	0.93	3.56	0.93	5.45	3.69	4.68	0.52
Zr	66	77	127	115	95	116	194	91	47	104	107	99	71	100
Hf	2.16	2.60	1.40	1.76	1.99	3.20	4.68	3.09	1.53	3.09	1.56	1.37	1.79	1.77
Th	7	10	5	8	9	8	9	8	7	8	7	7	9	5
Nb	8	11	6	6	8	8	8	7	6	7	6	10	8	9
Pb	14	21	14	29	43	28	24	20	41	34	28	24	34	13
Y	28	36	23	27	26	27	28	26	24	28	29	30	26	41
Cr	36	34	21	20	57	34	18	10	13	18	8	19	16	23
Ni	13	15	18	15	15	14	8	11	17	12	13	14	13	6
Co	23	15	18	19	20	20	14	21	23	21	21	18	24	11
V	181	155	156	163	154	161	104	185	191	185	172	185	162	162
Zn	76	59	56	96	85	75	64	51	53	55	51	80	77	28
La	20.40	27.80	22.02	23.40	20.01	22.10	30.60	23.50	19.40	18.40	22.80	23.02	21.90	21.10
Ce	43.40	55.40	42.10	48.20	41.10	45.50	62	48.50	37.30	40.80	46.56	47.30	44.60	44.80
Pr	5.41	7.15	5.10	5.87	5.12	5.45	7.15	5.93	4.34	5.26	5.77	5.80	5.41	5.75
Nd	21.80	29.20	21.10	23.11	20.70	21.2	27.2	23.20	17.20	21.80	23	22.80	21.30	24.10
Sm	4.84	6.74	4.80	4.92	4.60	4.57	5.39	4.83	3.71	4.98	5.03	5.02	4.60	6.02
Eu	1.07	1.26	1.20	1.20	1.11	1.20	1.08	1.29	1.01	1.32	1.25	1.10	1.11	1.07
Gd	4.81	6.30	4.58	4.71	4.55	4.41	5.09	4.43	3.65	4.87	4.94	4.87	4.37	6.21
Tb	0.76	1.02	0.72	0.74	0.70	0.70	0.79	0.66	0.57	0.75	0.74	0.75	0.69	1.05
Dy	4.82	6.34	4.50	4.51	4.42	4.46	4.78	4.10	3.69	4.72	4.70	4.72	4.22	6.87
Ho	0.99	1.28	0.96	0.92	0.90	0.92	0.97	0.83	0.74	0.96	0.94	0.96	0.87	1.41
Er	2.98	3.77	2.70	2.78	2.69	2.78	2.94	2.44	2.29	2.87	2.79	2.87	2.57	4.34
Tm	0.43	0.54	0.43	0.39	0.38	0.40	0.42	0.35	0.33	0.42	0.39	0.42	0.36	0.63
Yb	2.89	3.62	2.75	2.66	2.58	2.74	2.84	2.29	2.29	2.75	2.52	2.75	2.49	4.31
Lu	0.43	0.54	0.43	0.39	0.38	0.41	0.43	0.35	0.35	0.41	0.38	0.41	0.37	0.64
(Gd/Yb)cn	1.34	1.40	1.34	1.43	1.42	1.30	1.45	1.56	1.29	1.41	1.58	1.43	1.42	1.16
(La/Yb)cn	4.76	5.18	5.39	5.93	5.23	5.44	7.26	6.92	5.71	4.40	6.09	5.64	5.93	3.28
Eu/Eu*	0.68	0.59	0.78	0.76	0.74	0.82	0.63	0.85	0.84	0.81	0.77	0.68	0.76	0.53

Rock types: gr granite, grd granodiorite, tn tonalite, mz monzonite, dio diorite, mz.dio monzodiorite, gbb.dio gabroic diorite, +mafic microgranular enclave. ASI is the aluminum saturation index [molar $Al_2O_3/(CaO+K_2O+Na_2O)$]. Mg# is $100\times MgO/(MgO+0.9FeO_{tot})$ in molar proportions. Oxides are given in wt.%, trace elements in μg/g.

host rocks. Oxygen fugacities (log fO_2), estimated using the model by Spencer and Lindsley (1981), vary between −20.5 to −16.1 (host rocks) and −20.8 to −15.8 (MMEs). All samples show relatively low fO_2 and are plotted just above the nickel–nickel oxide (NNO) buffers modified by the solution model of Frost (1991) (not shown). The fugacity features of the plutons are consistent with those proposed by Aydin et al. (2003) if their biotite compositions are used.

4.3. K–Ar dating

Four biotite separates from the plutons were used for a K–Ar age determination. All the biotite samples (Id2a, D10, Ah2 and Is5) are fresh and expected to give reliable ages to represent the cooling histories of the plutons. The separates yield K–Ar ages ranging from 42.7±2.21 to 44.1±2.22 Ma (Table 5). The biotite ages correspond to the time of biotite cooling to its blocking temperature at about 345–310 °C (e.g. Grove and Harrison, 1996). Therefore, the biotite cooling age of ~43 Ma (Lutetian) is interpreted as an approximation for the intrusion age.

4.4. Major and trace elements

Representative chemical analyses are listed in Table 6. In the classification diagram of Middlemost (1994), the host rocks from the plutons plot in the fields of granite, granodiorite, tonalite, monzonite and diorite and their MMEs in the fields of gabbroic diorite, diorite and monzo diorite (Fig. 5). The host rocks are metaluminous to slightly peraluminous with ASI [=molar $Al_2O_3/(CaO+K_2O+Na_2O)$] ranging from 0.82 to 1.09 and are of I-type character while the MMEs are only metaluminous (ASI=0.75–0.86) (Fig. 6A). All samples are of subalkaline affinity and belong to calc-alkaline and high-K calc-alkaline series, which are greatly predominant (Fig. 6B). They are close to the boundary marked by the line $\sigma=2.5$, suggesting the presence of high-K calc-alkaline character (Fig. 5). Major and trace element variations are shown in Harker plots (Fig. 7). The MMEs and their host rocks display a wide range in SiO_2 content, but the MMEs (with SiO_2=53–61%; mostly <57%, Mg#=44–54) are less differentiated than the host rocks (with SiO_2=57–73%, Mg#=37–50; Table 6). All the rocks define a similar variation trend without a compositional gap in most of the Harker plots (Fig. 7A–P). Al_2O_3, MgO, Fe_2O_3, CaO, TiO_2 and P_2O_5 contents linearly increase with decreasing SiO_2, while K_2O decreases and Na_2O is nearly constant. Strong correlations between some major oxides and SiO_2 suggest significant fractionations for some of the mafic and felsic phases during the magma evolution. The host rocks have chemical composition slightly different than those of the MMEs, with lower CaO, MgO, Al_2O_3 and higher Fe_2O_3, K_2O and Na_2O. Similarly, the MMEs show higher Co, Sr and lower Ba, Hf, Yb, Rb than their respective host rocks (Table 6; Fig. 7) whereas Nb and Nd contents are nearly similar. All the samples exhibit rather similar trace element abundance patterns, with enrichment in large ion lithophile (LIL) elements (e.g. Cs, Rb, Th, K, Rb, Ba and Sr) and strongly pronounced negative anomalies in HFS elements such as Ti and Nb compared to the primitive mantle (Fig. 8A, B). Chondrite-normalized REE

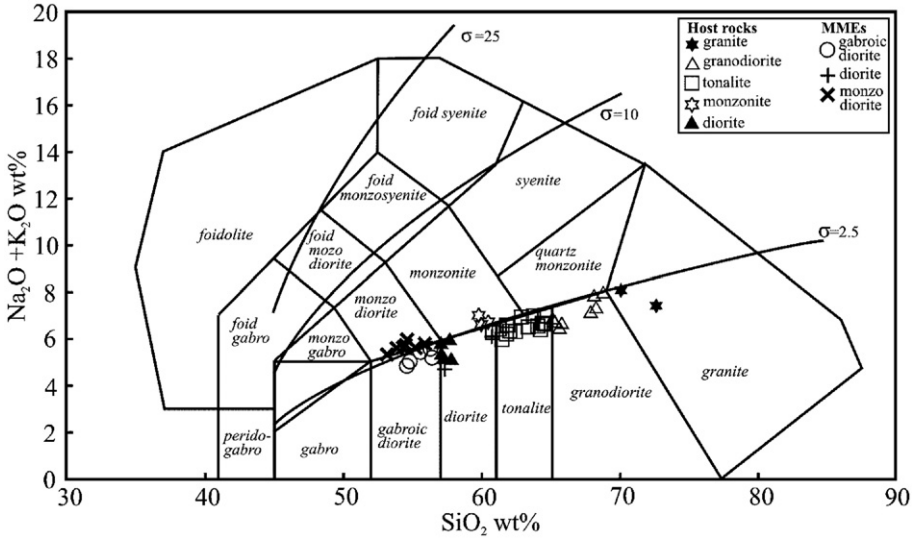

Fig. 5. Classification diagram (Middlemost, 1994) for the Dölek and Sariçiçek plutons. σ is a Rittmann index, defined as $(K_2O+Na_2O)^2/(SiO_2-43)$.

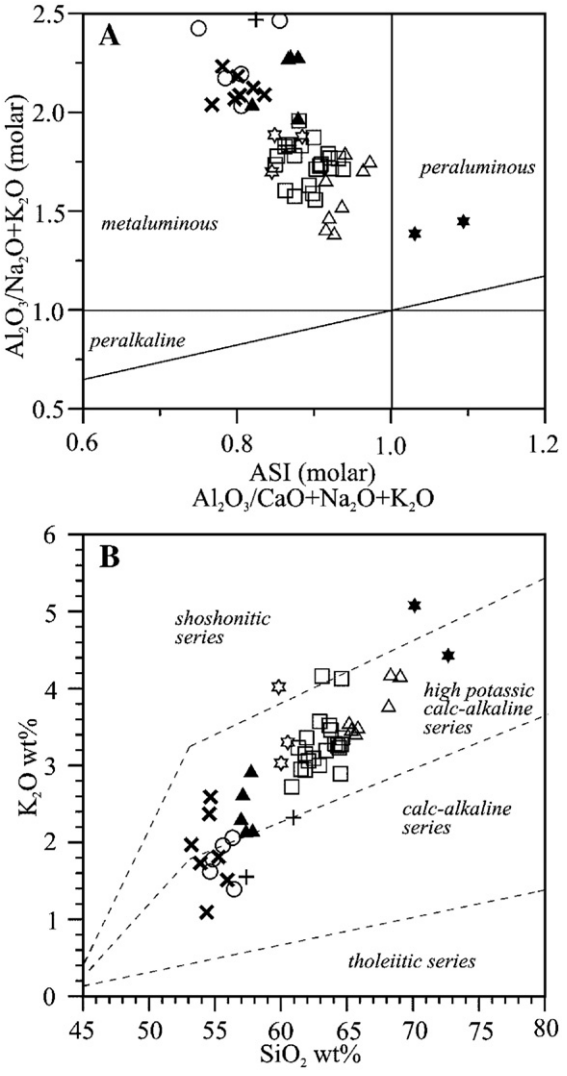

Fig. 6. Chemical variation diagrams for the Dölek and Sariçiçek plutons illustrating some chemical features that distinguish between the granitoid rocks. (A) Al_2O_3/Na_2O+K_2O (molar) versus ASI (after Maniar and Piccoli, 1989) diagram for the plutons. (B) K_2O versus SiO_2 diagram for the samples with lines separating tholoiitic, calc-alkaline, high-K calc-alkaline and shoshonitic series of Peccerillo and Taylor (1976).

patterns are plotted in Fig. 9A, B. The REE abundance patterns of the samples are all characterized by a fractionation between light and heavy REEs. The host rocks display more fractionated REE pattern ([La/Yb]cn = 5–8 and [Gd/Yb]cn = 1.26–1.58), with heavy flatter REE patterns than their mafic enclaves ([La/Yb]cn = 4–7 and [Gd/Yb]cn = 1.16–1.58) (Fig. 8A, B; Table 6). All the samples have small negative Eu anomalies (host rocks; Eu/Eu* = 0.62–0.88, MMEs; Eu/Eu* = 0.53–0.85). The Dölek and Sariçiçek plutons are characterized by very low abundances of high-field strength (HFS) elements (Nb, Hf and Zr). In particular, their Nb (~ 8 ppm) is lower than the average value of I-type granites (21 ppm) as described by Chappell (1999) for the Lachlan Belt. The plutons have Rb, Sr, Ba, Yb, Y and Nb abundances similar to several other post-collisional granitoids such as those in the northern zone of the Pontides (Boztuğ et al., 2006), in the Central Aegean area (Altherr and Siebel, 2002) and in the Junggar Terrane of NW China (Chen and Jahn, 2004). Of particular significance is that the Dölek and Sarıçiçek plutons appear to have higher Y content and lower $(La/Yb)_{cn}$ values than those of the Saraycik pluton with adakite-like signature, which is located in the southern zone of the Pontides (Topuz et al., 2005).

4.5. Sr–Nd–Pb isotopes

Granitic samples for the Nd–Sr–Pb isotope analyses given in Tables 7 and 8 were selected in a way that covers the entire range of the compositional spectrum of the host rocks and mafic enclaves, that is, from the most primitive rock types to the most evolved ones. Initial Nd–Sr isotopic compositions were calculated at the age of 43 Ma. Regardless of rock types and SiO_2 content, the host rocks from Dölek and Sariçiçek plutons display relatively homogeneous isotopic compositions of I_{Sr}(43 Ma) ranging from 0.70482 to 0.70548 and of ε_{Nd}(43 Ma) from −0.6 to 0.8. The corresponding Nd model ages (T_{DM}) are in the range 0.84–0.99 Ga. The MMEs show I_{Sr} (0.70485–0.70517) and ε_{Nd}(43 Ma) values (−0.1 to 0.8) similar to the respective host rocks, but the Nd model ages (T_{DM} = 0.86–1.36 Ga) are slightly older than the host rocks. Lead isotopic ratios of the host rocks are ($^{206}Pb/^{204}Pb$) = 18.60–18.65, ($^{207}Pb/^{204}Pb$) = 15.61–15.66, ($^{208}Pb/^{204}Pb$) = 38.69–38.85, which are similar to those of the MMEs [($^{206}Pb/^{204}Pb$) = 18.58–18.64, ($^{207}Pb/^{204}Pb$) = 15.60–15.66, ($^{208}Pb/^{204}Pb$) = 38.64–38.77]. North hemisphere reference line (NHRL) was used in the plots since ^{208}Pb data is more radiogenic than ^{206}Pb. Also plotted for comparison are EM1 (enrich mantle with intermediate $^{87}Sr/^{86}Sr$, low $^{143}Nd/^{144}Nd$ and low $^{206}Pb/^{204}Pb$) and EM2 (enrich mantle with high $^{87}Sr/^{86}Sr$, intermediate $^{143}Nd/^{144}Nd$ and high $^{206}Pb/^{204}Pb$; Zindler and Hart, 1986). All the samples are very homogeneous in lead isotopic compositions (Fig. 10A, B) and plot between EM1 and EM2 although closer to EM2 that points out an interaction process between EM1 and EM2 components for their genesis.

In order to reveal their source properties, we plot the initial $^{143}Nd/^{144}Nd$ ratios (expressed as $\varepsilon_{Nd}(t)$ values) against I_{Sr}. All rocks plot to the right of the mantle array in

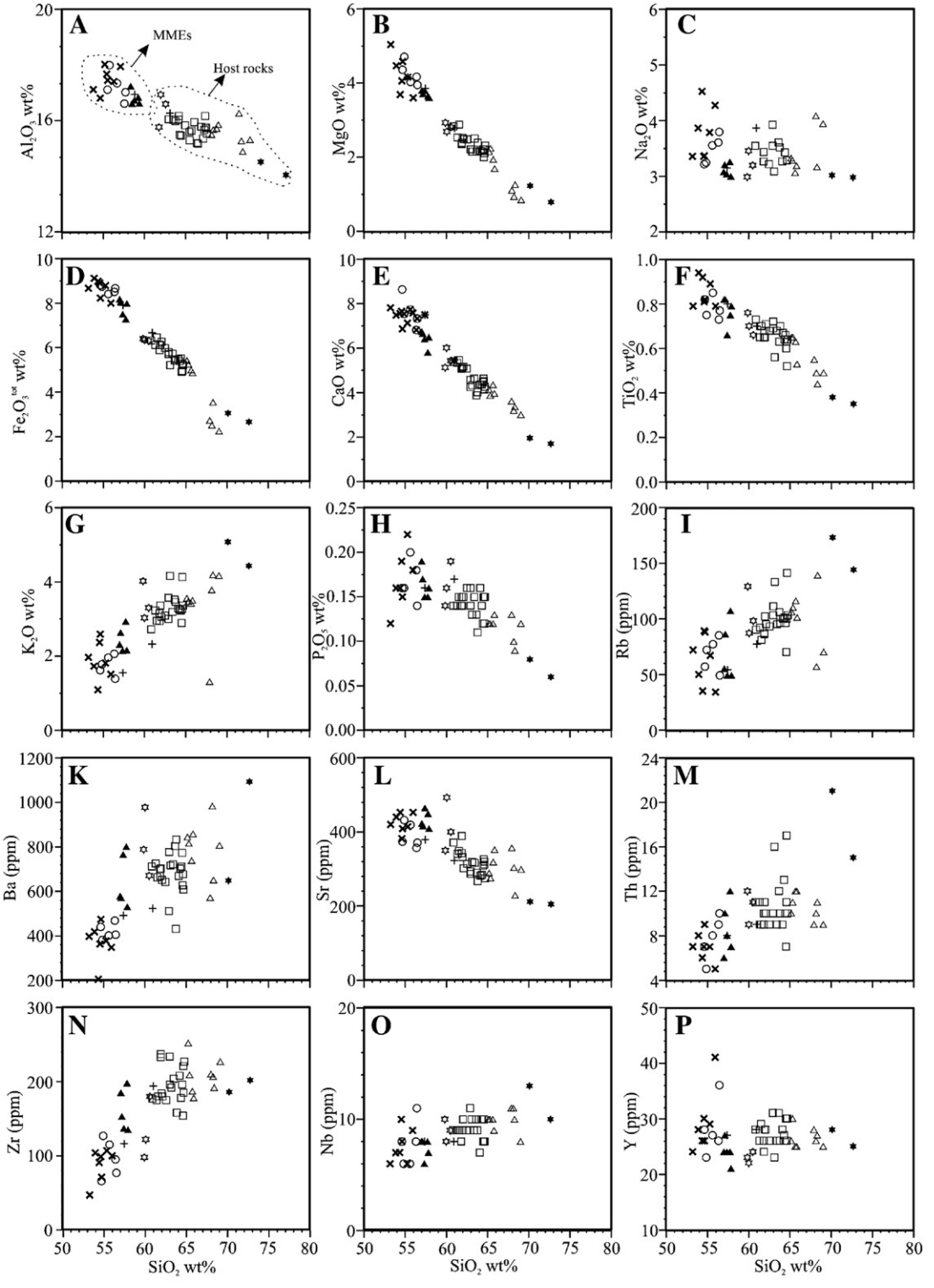

Fig. 7. (A–P) Harker variation diagrams for the samples from the plutons.

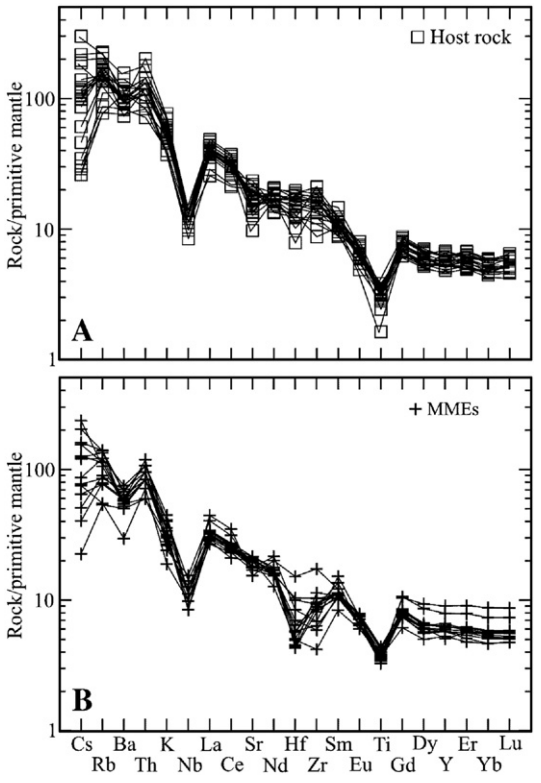

Fig. 8. (A–B) Primitive mantle-normalized multi-element variation patterns (normalized to values given in Sun and McDonough, 1989) for the Dölek and Sariçiçek plutons.

Fig. 10A and show a negative correlation between ε_{Nd} (43 Ma) values and I_{Sr}(43 Ma) ratios. Such a correlation is generally attributed to a magma interaction between crustal and mantle sources (e.g. Parada et al., 1999; Chen et al., 2002).

5. Discussion

5.1. General considerations and hypothetical genetic model

The hybrid host rocks from the Dölek and Sariçiçek plutons have a wide range of silica content (SiO_2=57–72 wt.%) and relatively high Mg# (37 to 50). It appears unlikely that felsic magmas were derived from basaltic parent magma by fractional crystallization or AFC process, as is also proposed by Grove and Donnelly-Nolan (1986) and Han et al. (1997), because the host rocks have SiO_2 content >57 wt.% and none of them are of basaltic composition in the area. That is, if the latter process took place during the generation of the felsic rocks, then the basic rocks would be much more abundant than the felsics. Such felsic magmas (SiO_2=57–72 wt.%; Mg#=37–50) could not be generated by the differentiation of the mantle-derived mafic magmas. Furthermore, Sr–Nd–Pb isotopes alone cannot be accounted for the mantle-derived mafic magma; some involvements of crustal melts in the source are needed. The MMEs of the plutons are also characterized by relatively low silica content (53–60%, mostly <57%) and relatively high Mg# (45–54) and could not originate from the partial melting of the lower crust due to the low silica content (~53%) and relatively high Mg#. The samples would be very low in Mg# if the granitoid magmas were derived from the partial fusion of such isotopically similar crustal rocks. Therefore, a mantle contribution is required in their genesis. In addition, high-K magmas were interpreted to originate from a mantle source (e.g. Soesoo, 2000) or a mixture between mantle magma and crustal melts (e.g. Ferré and Bernard, 2001). The I_{Sr} (43 Ma) ratios (>0.705) are inconsistent with a mantle derivation for high-K magmas.

We propose a magma interaction model for the origin of the plutons, as is summarized below. Intrusion of the mantle-derived mafic magma into the lower continental crust, which carries the necessary heat source for the

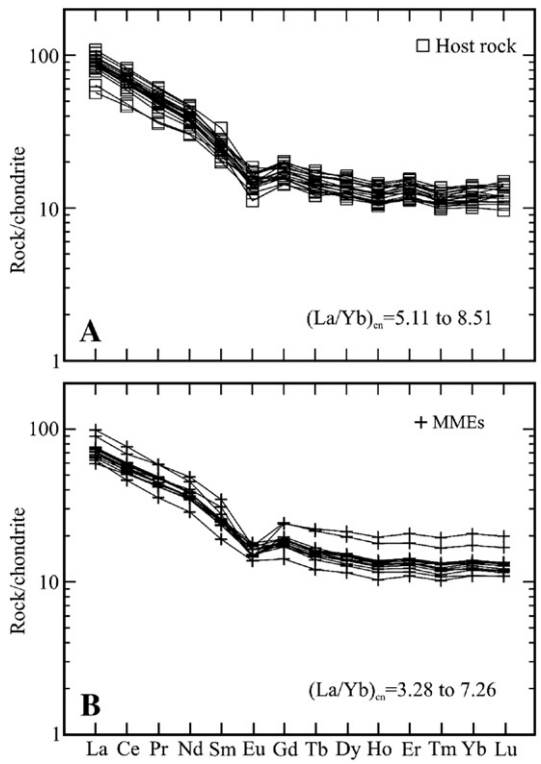

Fig. 9. (A–B) Chondrite-normalized (to values given in Boynton, 1984) rare earth element abundance patterns for the selected samples from the plutons.

Table 7
Rb–Sr and Sm–Nd isotope compositions for the rocks from the plutons

Sample	[Rb] ppm	[Sr] ppm	$^{87}Rb/^{86}Sr$	$^{87}Sr/^{86}Sr$	$2\sigma m$	I_{Sr} (43 Ma)	ε_{Sr}(T) (43 Ma)	[Sm] ppm	[Nd] ppm	$^{147}Sm/^{144}Nd$	$^{143}Nd/^{144}Nd$	$2\sigma m$	$\varepsilon_{Nd}(0)$	ε_{Nd}(T) 43 Ma	$f_{Sm/Nd}$	T_{DM} (Ga)
Host rocks																
Sr11	138.40	202.70	1.9563	0.706679	12	0.70548	15.00	4.212	22.14	0.1152	0.512587	13	−1.0	−0.6	−0.41	0.87
Er2	21.17	359.20	0.1691	0.705558	10	0.70545	14.70	6.047	30.66	0.1194	0.512592	13	−0.9	−0.5	−0.39	0.90
Sr38	95.92	274.60	1.0033	0.705852	13	0.70524	11.60	5.032	24.09	0.1265	0.512594	13	−0.9	−0.5	−0.36	0.97
Id2a	124.20	348.60	1.0264	0.705446	13	0.70482	5.67	4.779	22.76	0.1271	0.512658	13	0.4	0.8	−0.35	0.87
Ed12	50.90	412.80	0.3596	0.705321	13	0.70510	9.59	4.355	19.65	0.1341	0.512663	12	0.5	0.8	−0.32	0.93
Id5	40.96	385.10	0.6765	0.705419	12	0.70501	8.48	4.769	23.44	0.1232	0.512653	10	0.3	0.7	−0.37	0.84
Id17	81.00	375.20	0.6197	0.705531	12	0.70515	10.39	4.200	20.01	0.1271	0.512611	13	−0.5	−0.1	−0.35	0.95
Id1c	64.64	293.40	0.6304	0.705550	14	0.70516	10.65	4.186	21.04	0.1204	0.512619	11	−0.4	0.0	−0.39	0.87
Is4	86.19	312.10	0.7929	0.705684	8	0.70520	11.05	4.752	22.53	0.1277	0.512599	12	−0.8	−0.4	−0.35	0.98
MMEs																
Id5+	32.05	450.70	0.2038	0.705128	10	0.70500	8.29	4.757	22.76	0.1265	0.512657	12	0.4	0.8	−0.36	0.86
Id10+	76.93	341.20	0.6481	0.705374	12	0.70498	10.88	4.656	20.27	0.1391	0.512664	20	0.5	0.8	−0.29	0.99
Id17+	45.90	421.40	0.3125	0.705366	12	0.70517	6.00	5.189	22.38	0.1404	0.512608	12	−0.6	−0.3	−0.29	1.13
Id1c+	30.72	433.60	0.2044	0.705970	11	0.70485	10.36	6.187	24.16	0.1550	0.512628	9	−0.2	0.0	−0.21	1.36
Is4+	48.82	373.10	0.3761	0.705379	13	0.70515	7.65	4.687	21.46	0.1322	0.512616	13	−0.4	−0.1	−0.33	1.00
Id11+	65.50	433.10	0.4342	0.705224	12	0.70496	7.86	4.602	21.28	0.1309	0.512660	13	0.4	0.8	−0.34	0.90

Note: $\varepsilon_{Nd}=((^{143}Nd/^{144}Nd)_s/(^{143}Nd/^{144}Nd)_{CHUR}-1)\times 10{,}000$, $f_{Sm/Nd}=(^{147}Sm/^{144}Sm)_s/(^{147}Sm/^{144}Sm)_{CHUR}-1$, $(^{143}Nd/^{144}Nd)_{CHUR}=0.512638$, and $(^{147}Sm/^{144}Sm)_{CHUR}=0.1967$. The model ages were calculated using a linear isotopic ratio growth equation:
$T_{DM}=1/\lambda\times\ln(1+((^{143}Nd/^{144}Nd)_s-0.51315)/((^{147}Sm/^{144}Nd)_s-0.2137))$.

Table 8
Lead isotopic analyses for the granitoidic rocks from the Dölek and Sariçiçek plutons

Sample	$^{206}Pb/^{204}Pb$	2σm	$^{207}Pb/^{204}Pb$	2σm	$^{208}Pb/^{204}Pb$	2σm
Host rocks						
Sr11	18.6110	0.006	15.6101	0.006	38.6931	0.006
Er2	18.6015	0.004	15.6367	0.005	38.7572	0.004
Sr38	18.6057	0.007	15.6050	0.007	38.6823	0.007
Id2a	18.6512	0.015	15.6589	0.015	38.8509	0.016
Ed12	18.5868	0.007	15.6255	0.007	38.6802	0.008
Id5	18.6320	0.008	15.6222	0.009	38.7170	0.009
Id17	18.6026	0.014	15.6200	0.015	38.7006	0.016
Id1c	18.6524	0.017	15.6453	0.017	38.8505	0.017
Is4	18.5809	0.009	15.6268	0.009	38.6862	0.009
MMEs						
Id5+	18.6414	0.010	15.6240	0.009	38.7124	0.010
Id10+	18.5819	0.007	15.6182	0.007	38.6450	0.007
Id17+	18.6027	0.011	15.6558	0.010	38.7610	0.011
Id1c+	18.5807	0.006	15.6151	0.006	38.6458	0.006
Is4+	18.5863	0.007	15.5996	0.008	38.6431	0.007
Id11+	18.6006	0.010	15.6574	0.010	38.7677	0.010

dehydration melting of the lower crust (e.g. Rushmer, 1991; Rapp and Watson, 1995; Pedford and Gallagher, 2001) generates the granitic melts. Wyllie and Wolf (1993), Wolf and Wyllie (1994), and Lopéz and Castro (2001) experimentally showed that amphibolites start to melt at relatively high temperatures (800 to 900 °C) at pressures <1 GPa, whereas dehydration melting commences at temperatures as low as 750 °C, at ~1 GPa. In addition, the melt composition resulting from the partial melting of the mafic lower crust are controlled by the water content, source composition, degree and *P–T* conditions of the melting (e.g. Rapp et al., 1991; Şen and Dunn, 1994; Wolf and Wyllie, 1994; Rapp and Watson, 1995; Winther, 1996; Lopéz and Castro, 2001). Recent experimental data have shown that regardless of the degree of the partial melting, the partial melting of the mafic lower crust could generate melts of metaluminous granitic composition (e.g. Rushmer, 1991; Tepper et al., 1993; Roberts and Clemens, 1993; Wolf and Wyllie, 1994; Rapp and Watson, 1995).

Interaction of subsequent granitoidic melts and mantle-derived mafic magma resulted in a hybrid parental magma that experienced a fractional crystallization process en route to the higher crustal levels generating the whole spectrum of granitoidic rocks in the area. The interaction process is clearly evidenced by the inversely correlated I_{Sr}(43 Ma) ratios and ε_{Nd}(43 Ma) values in Fig. 10A in which most of the samples plot between crust and mantle components. It is remarkable that analytical uncertainty for ε_{Nd} is less than 0.5 units, so the variation range of over 2 units of ε_{Nd} shown by these samples very likely suggests a hybridization process between two magmas with different isotopic compositions. The model is also supported by the evidences discussed below.

5.2. Fractional crystallization

Fractional crystallization is a plausible mechanism to explain the generation of a wide variety of rock types. The decreases in Al_2O_3, MgO, CaO, Fe_2O_3 and TiO_2 and increases in ASI, K_2O and Rb with the increase of SiO_2 are in agreement with the evolution of hybrid host rocks and MMEs by fractional crystallization (Figs. 6A and 7). With increasing SiO_2 content, the decrease of TiO_2 is related to titanite, ilmenite and magnetite fractionations,

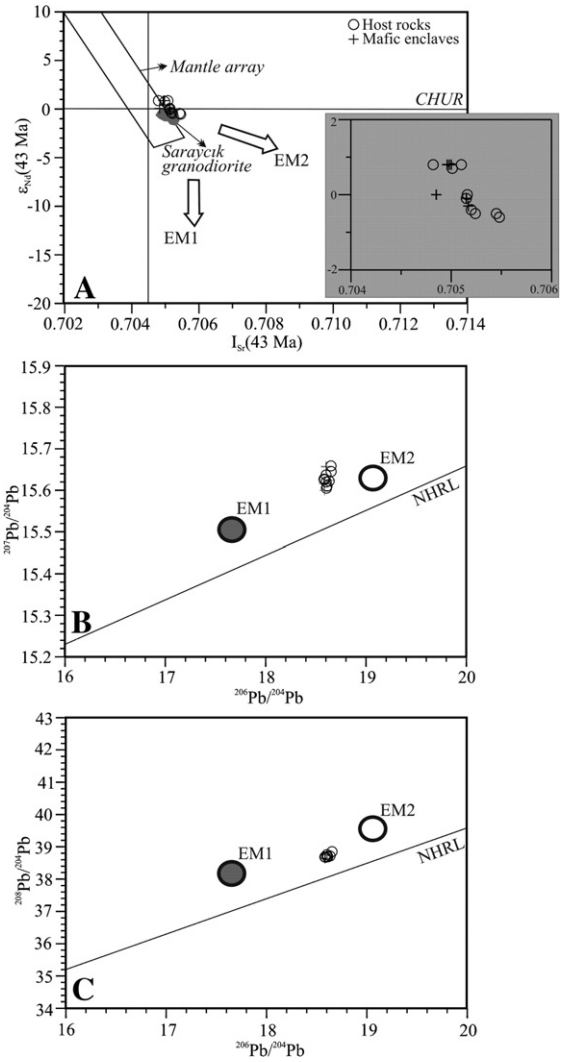

Fig. 10. (A) Plot of I_{Sr}(43 Ma) versus ε_{Nd}(43 Ma) values. (B–C) plots of $^{207}Pb/^{204}Pb$ versus $^{206}Pb/^{204}Pb$ and $^{208}Pb/^{204}Pb$ versus $^{206}Pb/^{204}Pb$ for the selected samples from the plutons.

while the decrease of P_2O_5 is regarded as a result of apatite fractionation. The negative Ti anomalies in spidergrams are consistent with titanite fractionation. The Ti anomalies may have also been caused by crustal contamination. However, the correlation of I_{Sr}(43 Ma) versus SiO_2 suggests that the crustal contamination is not a major evolution process in the genesis of rocks, as is discussed below. Also, the fractionation of the accessory phases such as zircon and titanite is recorded by the depletion in zirconium and yttrium. The negative CaO, Fe_2O_3 and MgO correlations with SiO_2 may also reflect on the pyroxene fractionation. The hybrid host rocks and their MMEs are characterized by high CaO and Sr contents and have small Ba, Sr and Eu negative anomalies (Figs. 8 and 9), suggesting that plagioclase fractionation has played a role in the genesis. These geochemical features along with their mineralogy are in agreement with a genetic relationship between the least and most evolved products of the plutons. Considering all the data together, it is possible to say that the fractional crystallization has also modified the chemical compositions of the plutons.

The fractional crystallization process for the plutons was modeled by a least-squares method for the major elements. The compositions of plagioclase, amphibole, biotite and Fe–Ti oxides used in the models are microchemical analyses of minerals from the rocks of the plutons. The calculations were performed based on the average composition of the gabbroic diorite (MME) and diorite as parent, and diorite and granite as daughter from the plutons. Two stages of the crystal fractionation were calculated: (1) formation of diorite (host rock) from gabbroic diorite (MME); (2) formation of granite from diorite. The results of calculations are given in Table 9. Most solutions represented here have sums of squared residuals less than 1. The first calculation (stage 1) demonstrates that dioritic host rocks could be produced from the parental magma by fractionation of 32% plagioclase, 16% amphibole, 5% biotite and 3% Fe–Ti oxides. The proportion of the melt remaining is 43 wt.%. To produce the granite daughter from the diorite magma (stage 2), extractions of lesser amount (in total of ~46 wt.%) of plagioclase, amphibole, biotite and Fe–Ti oxides are necessary (Table 8). For both stages 1 and 2 the residual sums of squares are 0.04 and 0.10, respectively, implying that the crystallizing mineral phases and their proportions were reasonably predicted. The proportion of minerals fractionated seems realistic, considering the modal mineral composition of the rocks. Also, the fractionation modeling shows that the crystal fractionation is a plausible mechanism to produce a wide variety of rock types from the plutons. Additionally, the Nd–Sr isotopic data of the hybrid rocks are all identical within the error limits (Table 7). We suggest that the magmatic evolution of the rocks has followed essentially a closed system fractional crystallization whereas an open system process is expected in the case of clear distinction in the isotopic compositions between all the rock compositions.

Although fractional crystallization is considered as one of the predominant processes, the whole-rock and

Table 9
Major element oxides fractional crystallization modeling for the hybrid rocks of the plutons

	Stage 1: Gabbroic diorite (e)–Diorite (h)			Stage 2: Diorite (h)–Granite (h)		
	Parent	Daughter		Parent	Daughter	
	Average (n=7)	Observed (n=6)	Calculated	Average (n=6)	Observed (n=2)	Calculated
SiO_2	55.67	59.17	59.24	59.17	71.92	71.96
TiO_2	0.84	0.77	0.59	0.77	0.37	0.30
Al_2O_3	17.63	17.06	17.20	17.06	14.37	14.43
FeO^t	8.02	6.94	7.01	6.94	2.58	2.62
MgO	4.38	3.67	3.82	3.67	1.01	1.07
CaO	7.88	6.36	6.33	6.36	1.86	1.88
Na_2O	3.72	3.20	3.08	3.20	3.02	2.97
K_2O	1.68	2.67	2.66	2.67	4.79	4.83
P_2O_5	0.16	0.16	0.09	0.16	0.07	−0.06
Fractionating	Plagioclase		32.35			28.59
Minerals, wt.%	Amphibole		16.81			13.96
	Biotite		4.51			0.04
	Fe–Ti oxides		2.94			2.96
Residual melt, wt.%			43.39			54.45
Sum residuals squared	(r^2)		0.04			0.10

Major elements are recalculated to total=100% volatile free, total Fe as FeO. Mineral compositions used for modeling are an average value of mineral compositions given in Tables 1, 2 and 3. e enclave, h host rock.

Nd–Sr isotopic data reveal that a small amount of assimilation/contamination plays some role in the genesis of the hybrid rocks. The effects of assimilation may be assessed by elemental and isotopic ratios. There does not appear a strong correlation between initial $^{87}Sr/^{86}Sr$ ratios or ε_{Nd}(43 Ma) and SiO_2 content (Fig. 11A, B) as one would expect if the crustal assimilation is a dominant petrogenetic process. But the plot of I_{Sr}(43 Ma) versus SiO_2 (Fig. 11B) suggests that lesser amount of crustal contamination, which is not a dominant petrogenetic process, combines with the effects of fractional crystallization during the emplacement of the hybrid magma in the crust.

5.3. Origin of mafic microgranular enclaves

Many workers now agree that the MMEs are formed by magma mixing and mingling processes, which are characteristics of calc-alkaline felsic intrusions (e.g. Vernon, 1984; Poli and Tommasini, 1991; Barbarin and Didier, 1992; Kumar et al., 2004). However, their origin is still controversial. In addition, the magma interaction

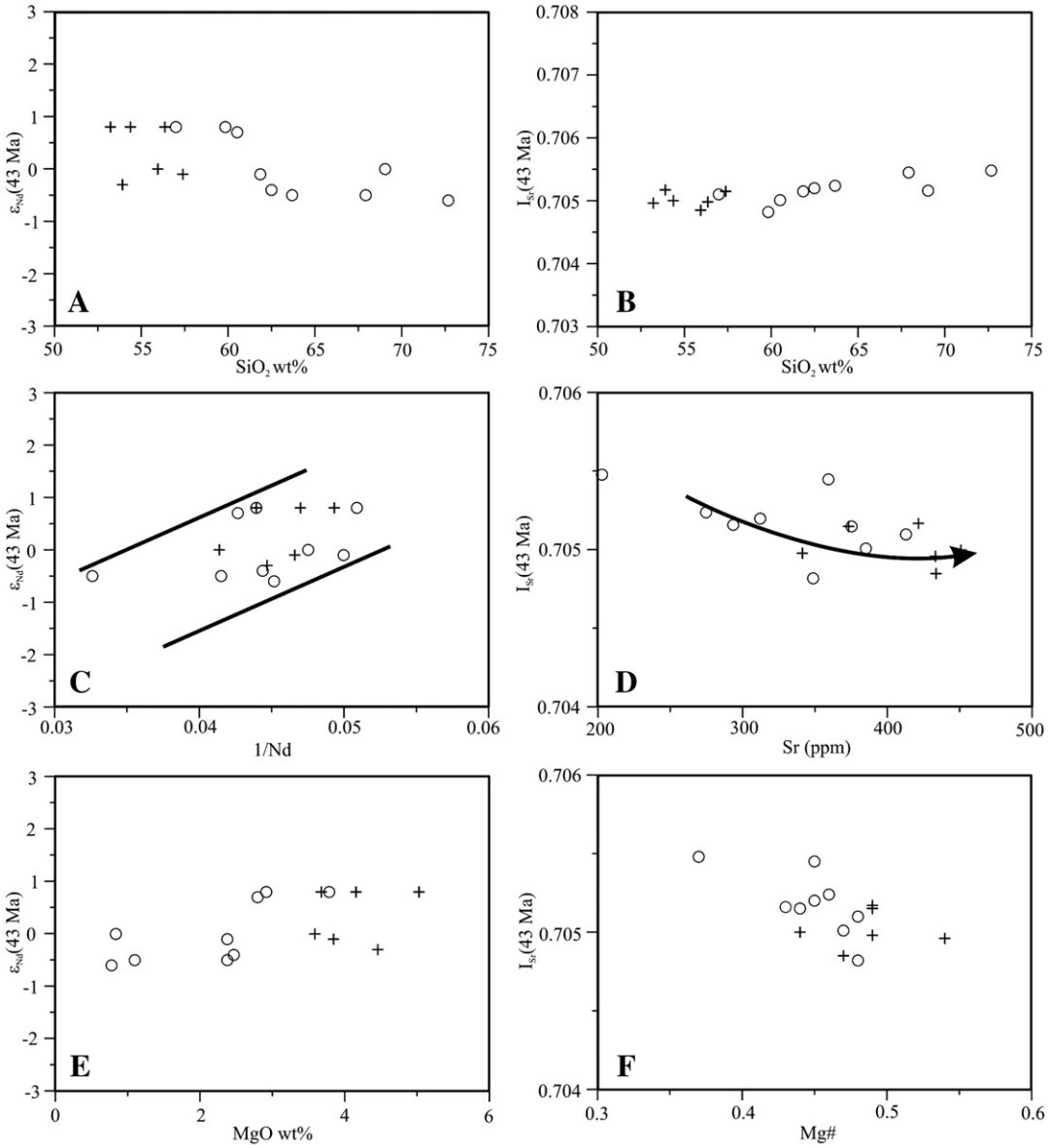

Fig. 11. (A–B) Silica versus ε_{Nd}(43 Ma) and I_{Sr}(43 Ma) plots and plots of (C) ε_{Nd}(43 Ma) versus 1/Nd, (D) I_{Sr}(43 Ma) versus Sr (ppm), (E) ε_{Nd}(43 Ma) versus MgO wt.% and (F) I_{Sr}(43 Ma) versus Mg# for the samples from the plutons.

has become the most common model to interpret the origin of the MMEs, with their finer grain sizes being attributed to the undercooling of a mafic magma in a cooler, felsic magma (e.g. Vernon, 1984; Wiebe, 1991; Barbarin and Didier, 1992; Perugini and Poli, 2000; Kumar et al., 2004). The MMEs from the plutons have mineral assemblages, chemical relationships and isotopic compositions similar to their host rocks. The similarities of Sr–Nd–Pb isotopic compositions in particular are evidenced by the fact that the MMEs are not solid residues of a partial melting that represents a restitic origin. This in fact agrees well with both mixed and cognate origins. However, Donaire et al. (2005) pointed out that the MMEs from the Los Pedroshes granodiorite have similar isotopic compositions with their host rocks, indicating that the MMEs and their host rocks formed from a coeval, cognate magma. Additionally, the occurrences of both rounded and diffuse contacts in the MMEs indicate that batches of magmas with large variability of viscosity existed in the same magmatic system (e.g. Nittmann et al., 1985; Perugini et al., 2004). In this scenario, the presence of rounded interfaces and development of diffuse contacts between the MMEs and their host rocks may point out that both processes of quenching of mafic magma and felsic magma heated by mafic magma played major roles in the generation of the MMEs in the dynamic magma chamber. Therefore, such petrographic features do not fit the crystal accumulation (cognate) processes. Furthermore, isotopic equilibrium has been achieved between the mafic enclaves and their host with the passing of time (e.g. Poli and Tommasini, 1991). Many workers (e.g. Pin et al., 1990; Holden et al., 1991; Elburg, 1996) have claimed partial or complete isotopic equilibration of the MMEs with their host. Experiments show that the isotopic equilibration advances faster than the chemical equilibration and Sr isotopic equilibrium is faster than that of Nd (e.g. Holden et al., 1987; Pin et al., 1990). Compared to the Nd, the Sr isotopic compositions of the host and enclaves are more likely to be equilibrated through diffusion exchange. Looking at the data set, the sample Id5+ (MME) exhibits very similar isotopic composition of I_{Sr}(43 Ma) (0.70500) with respect to the host rock (Id5=0.70501; Table 7), while their $^{143}N/^{144}Nd$ ratios are slightly different. The strong isotopic similarity should be interpreted as having the isotopic equilibrium process more or less complete. Although the major and trace element abundances of the MMEs and their host rocks are slightly different (Table 6), both of them display comparable variations without a chemical gap in most of the diagrams (Figs. 6 and 7). Such a chemical variation is interpreted in terms of a two-end-member interaction as the basic process for the genesis of enclaves and their hybrid host rocks (e.g. Barbarin and Didier, 1992; Wiebe et al., 1997; Perugini et al., 2003). In addition, there are two compelling textural arguments against cognate origin of the enclave. First, some of the MMEs contain large, rounded plagioclase phenocrysts, which are compositionally similar to those in the host rocks (Table 1; Fig. 4C, H). The low rheological contrasts between the two magmas allow crystal transfer from the host magma into the basic magma (e.g. Barbarin and Didier, 1992; Waight et al., 2000; Perugini et al., 2003). This consideration is in agreement with the rounded plagioclase phenocrysts set in the enclave matrix (Fig. 4C, H), suggesting a mechanical transfer of the mineral grains during the magma mixing of the basic and felsic magmas behaving as liquids in their histories. Second, biotite and amphibole contents in the MMEs as ferromagnesian phases are always much lower than 50 vol.%. High content ferromagnesian phases in the MMEs are cited as evidence of a cognate process (Donaire et al., 2005), since the mafic phases can nucleate more quickly than the quartz and feldspar and can be enriched in early crystallization products, as proposed by Weinberg et al. (2001). The studied MMEs seem not to agree with the cognate process. Therefore, we conclude that the MMEs must have formed by a magma interaction process, in view of the textural and chemical relationships, identical mineral compositions and similar isotopic compositions between the MMEs and their hybrid host rocks.

5.4. Magma genesis

As evidenced by the geochemical data presented above, the samples from the plutons are characterized by pronounced negative Ba, Nb and Ti anomalies in the spidergrams (Fig. 8A, B) and enriched in LILEs and LREEs, suggesting typical crustal melts. However, such features are not always associated with the crustal melts, but may reflect on the mantle enrichment events prior to melting, as proposed by Hawkesworth et al. (1993) and Rottura et al. (1998). In fact, this relative enrichment of the hybrid host rocks and their MMEs, with initial Sr–Nd ratios that could be inherited from a mafic magma, derived from the melting of a chemically enriched subcontinental lithospheric mantle source. The MMEs have relatively low silica content (53–60%, mostly <57%) and relatively high Mg# (45 to 53) that both point to a mantle-derived magma. In addition, dioritic sample Ed6 characterized by low SiO_2 content (57 wt.%) and relatively high Mg# (~50) may not have pure crustal origin. However, its low Ni (6–18 ppm)

and Cr (8–36 ppm) content relative to those of the unfractionated magmas (200–450, and >1000, respectively) suggest that a mafic magma underwent a significant fractionation of olivine, pyroxene and spinel prior to the interaction. In addition, the Al_2O_3 content (15.52–17.22 wt.%) is not consistent with the basic parent melts (Al_2O_3 <15 wt.%) in equilibrium with the mantle source, which is probably due to the fractionation of some Al-poor mafic phases such as olivine and orthopyroxene. This is evidenced by the REE fractionated patterns of the rocks. The weakly negative to slightly positive ε_{Nd}(43 Ma) values (−0.6 to +0.8), slightly depleted I_{Sr}(43 Ma) ratios (0.7048 to 0.7054), relative enrichments of LILEs (e.g. Rb, Ba, Sr, Th and K) and LREE (e.g. La, Ce) and depletion of HFSEs (e.g. Nb, Ti; pronounced negative anomalies) all accord with the melting of a chemically enriched SCLM, which probably predominated the generation of the hybrid rocks, as discussed below. Lead isotopic ratios of the samples also indicate an enriched mantle source (EM2; Fig. 10B, C) that can be considered as an end-member of the mixing process in the genesis. Probably, the SCLM was chemically enriched by fluids rich in LREEs and LILEs or melts derived from the dehydration of the down-going slab that contains Paleozoic arc rocks of the earlier tectonic processes. With these guidelines, it is likely that the SCLM played an important role in the genesis. That is, the parental magma to the entire intermediate rock spectrum is in fact a hybrid magma, but not a purely mantle-derived-basic magma. For a more felsic end-member the upper crust-derived magma seems less likely because of the low initial Sr–Nd isotopic ratios of the hybrid granitoid rocks. The most felsic sample Sr11 is characterized by high silica (~73 wt.%), relatively low Mg# (36) and moderate I_{Sr} (43 Ma) (0.70548), which would be consistent with the melts derived from the lower crust. In the light of isotopic and whole-rock data, the lower crust-derived magma appears more likely as more felsic component in the generation of the hybrid plutons. In addition, underplating of mantle-derived magma and its interaction with the lower crust-derived magma have been recognized as the most favorable mechanism for the generation of the hybrid magmas (e.g. Rudnick et al., 1986). As cited above, this mechanism seems probable as the experimental studies show that underplating magma could provide the necessary heat source for the dehydration melting (e.g. Rushmer, 1991; Rapp and Watson, 1995; Pedford and Gallagher, 2001) and produce the granitic melt (e.g. Rushmer, 1991; Tepper et al., 1993; Roberts and Clemens, 1993; Wolf and Wyllie, 1994; Rapp and Watson, 1995).

Considering the $(La/Yb)_{cn}$ and Yb_{cn} content, the studied plutons do not show adakitic signature. Topuz et al. (2005) suggests an origin of the dehydration melting of the mafic lower crust for the post-collisional Saraycik pluton from the Eastern Pontides. This difference is regarded as resulting from the residual mineralogy in the source during the melting of the crustal material. This could be interpreted as an amphibole-poor residue in the source, as is evidenced by the enrichment of the LREEs. Additionally, isotopic compositions of the Saraycik plutons indicate a mixing process evidenced by the lack of a linear trend in Fig. 10A and are slightly different from the studied plutons herein. This interpretation also suggests that a magma derived from the dehydration melting of the lower crust is not the only source for the genesis of the plutons. Topuz et al. (2005) also showed that the underplating mechanism could result granitic melt by the dehydration melting of the lower crust in the Eastern Pontides.

5.5. Magma interaction process

The hybrid granitoid rocks and the existence of the widespread mafic microgranular enclaves suggest an interaction process for the genesis. The interaction process is also supported by the disequilibrium texture such oscillatory plagioclase (Fig. 4E) in the hybrid rocks. As emphasized above, the MMEs are not cumulates and do not have a mixed origin and thus at least two separate magmas are required to explain their generation. The mixing process is in agreement with the significant overlap of the data points of the host rock and their MMEs in ε_{Nd}(43 Ma) versus I_{Sr}(43 Ma) plot (Fig. 10A). Furthermore, the plots of the isotopic variations against the elemental and oxide compositions are attributed to a magma interaction (e.g. Thirlwall and Jones, 1993; Chen et al., 2002; Chen and Arakawa, 2005). In plot of ε_{Nd}(43 Ma) versus 1/Nd, the MMEs and their host rocks display a linear array, which accords with a magma interaction process (Fig. 11C). The very irregular hyperbolic trend of the samples in the I_{Sr}(43 Ma) versus Sr plot also indicates an interaction process in the genesis (Fig. 11D). The linear relationships in plots of ε_{Nd} (43 Ma)-MgO wt.%, I_{Sr}(43 Ma)-Mg# support the consideration of the magma interaction (Fig. 11E, F). To explain the magma interaction process in the genesis of the plutons, we used the binary four-element diagrams presented by Hollanda et al. (2003). The defined hyperbolic arrays on Ti/Zr versus Rb/Sr and the linear trend on Ti/Zr versus Sr/Zr plots, both of which are expected for the interaction between the two distinct compositional end-members, are evidenced by a simple

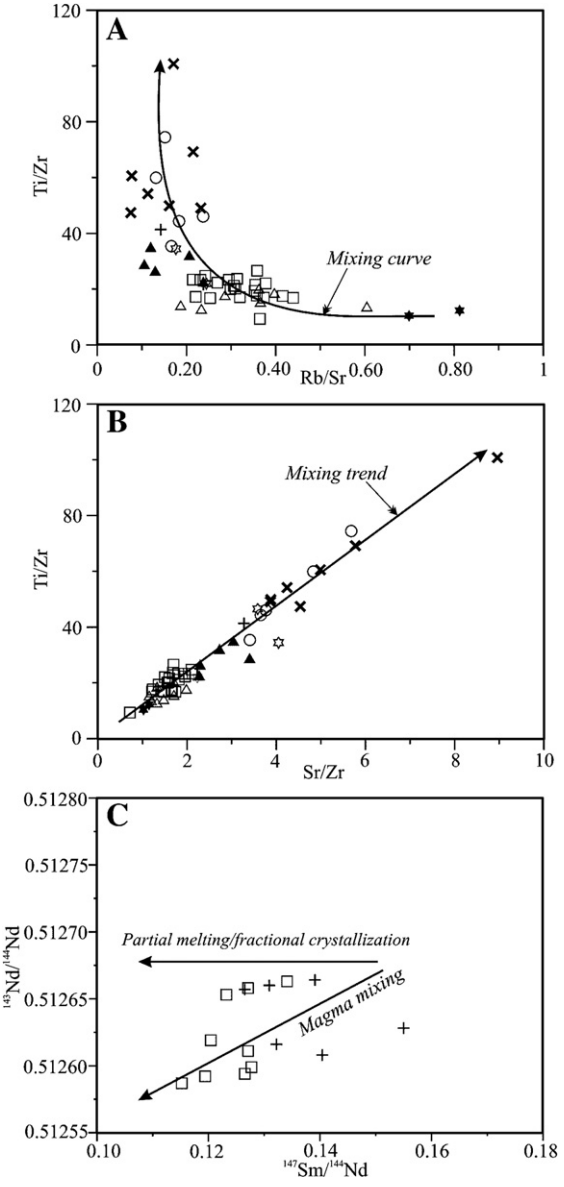

Fig. 12. (A–B) Interelement ratio plots, (C) $^{143}Nd/^{144}Nd$ versus $^{147}Nd/^{144}Nd$ diagram for the plutons.

interaction process of at least two magmas in the genesis (Fig. 12A, B). The binary diagram of $^{143}Nd/^{144}Nd$ versus $^{147}Sm/^{144}Nd$ (Fig. 12C) shows that the magma interaction process is a valid mechanism along with a fractional crystallization in the genesis of the hybrid rocks.

In order to better examine the interaction process, a modeling study was performed based on the AFC model of De Paolo (1981). In the modeling, the following assumption was made: the two-end-members are represented by average parent magma from the depleted mantle and by average lower continental crust. The Sr–Nd isotopic ratios and trace element concentration data explaining the modeling results are given in Fig. 13. Since the isotopic ratios of the lower crustal component for the Eastern Pontides are unknown, those values from Tibet (Chen and Jahn, 1998) are utilized. The isotopic trend corresponding to $r = \sim 0.3$ is shown by a curve in Fig. 13. Concerning the proportions of the incorporated end-members, the modeling results demonstrate that ~17–23% of the lower crust-derived magma may be incorporated with the mantle-derived mafic magma (~77–83%) in the generation of the hybrid granitoid rocks.

In summary, the petrological and geochemical data imply that at least two distinct magma bodies contributed to the genesis of the plutons. Underplating and intrusion of the mantle-derived hot basic magma into an already thickened continental crust could result in the dehydration melting of the lower crust. An extensive interaction between the lower crust-derived magma and mantle-derived melts (contributing ~77–83% to the mixture) has formed the large bodies of the hybrid magmas at depths. It is possible that the magma interaction process occurred at depths greater than 9 km, which is much deeper than the pluton depths estimated by the amphibole geobarometers. Then, the fractionation of the hybrid magmas en route to the upper crustal levels (~5–9 km below surface) has generated a variety of rock types ranging from diorite to granite in the southern part of the Eastern Pontides.

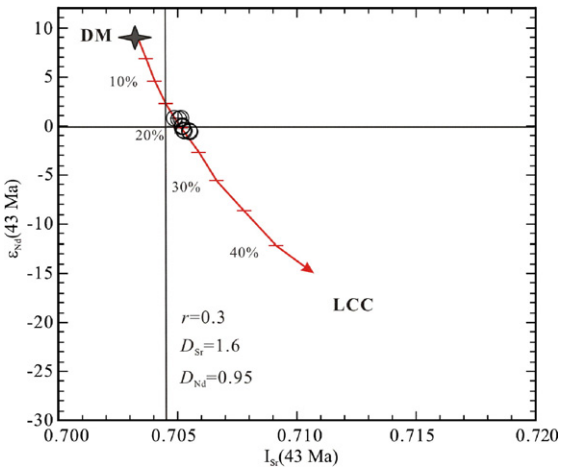

Fig. 13. Modeling diagram based on the AFC model of De Paolo (1981), showing a trend of Sr–Nd isotope variation as a result of magma interaction. The parameters used in the modeling are as follows: Lower continental crust (LCC): [Sr]=350 ppm, [Nd]=26 ppm, I_{Sr}=0.712, ε_{Nd}=−30. Parent magma from a depleted mantle (DM): [Sr]=530 ppm, [Nd]=24 ppm, I_{Sr}=0.703, ε_{Nd}=9.

6. Conclusions and geodynamic implications

On the basis of the integrated Sr–Nd–Pb, geochemical and geochronological analyses of the host rocks and their MMEs, the following scenario for the Dölek and Sariçiçek plutons from the Eastern Pontides could be outlined; the emplacement of the plutons, which are I-type and mostly metaluminous characteristics and belong to the high-K calc-alkaline series, took place at ~43 Ma (Lutetian) as revealed by the K–Ar ages on the biotite separates. Underplating is a well-known mechanism for the genesis of the hybrid granitoid rocks and is also adopted herein. It is believed that the timing of the underplating is closely related to the major episodes of the regional tectonics and also to the geodynamic processes in the deep parts of the subcontinental lithosphere. Cretaceous to Late Paleocene volcanic arc magmatism was formed as a result of the northward subduction of the northern branch of Neotethys (e.g. Şengör and Yilmaz, 1981; Okay and Şahintürk, 1997) (Fig. 14A). In 43 Ma (Lutetian), the underplated mantle-derived mafic magma possibly intruded into the Pontide continental crust, which was thickened by the earlier tectonic events. The collision between the Pontide continental crust and the Anatolide–Tauride block induced the thrust imbrications of the active margin, where the collision is dated back to Late Paleocene based on the ages of the foreland basin sequence in front of the north-vergent thrust sheets in the Eastern Pontides (e.g. Okay et al., 1997), as is summarized in Fig. 14B. This is consistent with the cessation of the arc magmatism in the region during the Late Paleocene (Elmas, 1995; Okay and Şahintürk, 1997). After the cessation of the collision event, the extentional period during Lutetian probably caused the upwelling of the asthenosphere that triggered

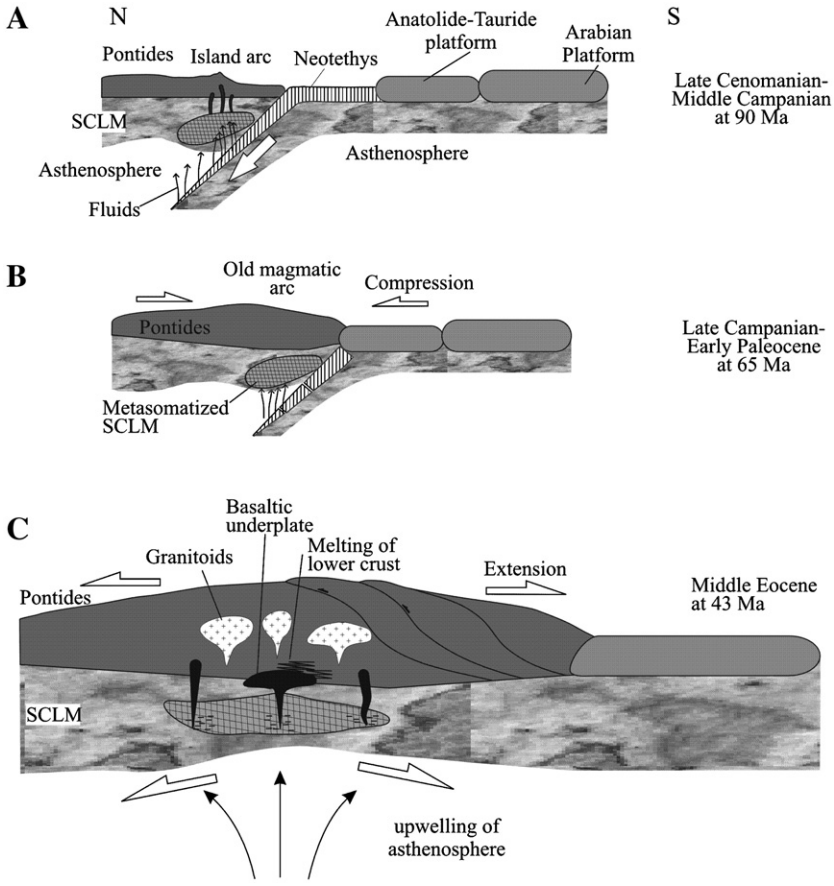

Fig. 14. Schematic illustration for the geodynamic evolution of the Eastern Pontides. (A) The eastern Pontide magmatic arc is interpreted as being formed during the northward subduction of the northern branch of Neotethys (Akin, 1979; Şengör and Yilmaz, 1981; Okay and Şahintürk, 1997). SCLM stands for subcontinental lithospheric mantle. (B) The collision of the Pontides and Anatolide–Tauride platform commenced at Late Campanian or Early Paleocene (Okay and Kelley, 1994; Okay and Şahintürk, 1997; Okay et al., 1997). (C) After the collision of the Pontide and Anatolide–Tauride platform, the thickened lithosphere underwent convective thinning (Houseman et al., 1981) leading to extentional magmatism in Middle Eocene.

the underplating of the mafic magma (Fig. 14C). Then, the intrusion of hot, chemically enriched SCLM-derived mafic magma induced the dehydration melting of the lower crust. An extensive interaction between the lower crust-derived melt and SCLM-derived magma, which were chemically enriched in incompatible elements (e.g. Rb, Ba, Sr and LREE) by fluids or melts derived from the dehydration of the old subducting slab (Fig. 14A, B) and depleted in the isotopic composition, produced the whole spectrum of the rock types ranging from diorite to granite in the upper crustal levels (~5–9 km below surface).

It is remarkable that the seismic velocity reversal (i.e. a low velocity zone) predicted by Çakir et al. (2000) and Çakir and Erduran (2004) for the lower crust depths beneath the seismic station TBZ, which has geographically close proximity to the current study area, is in good agreement with the lower crust melt mechanism needed to explain the geochemical data of the present study. It is a common perception that partial melting lowers the seismic velocities through reduction in strength. The magma underplating at seemingly lithospheric depths may also explain those disturbed seismic velocities observed by Çakir et al. (2000) and Çakir and Erduran (2004) for the subcrustal ranges.

Additionally, the Sr–Nd interaction modeling allowed more precise identification and even rough quantification of the two main source components (lithospheric mantle; 77–83% and lower crust; 17–23%), which are responsible for the magma genesis of the plutons. However, the Sr–Nd and geochemical data reveal that some minor contribution from the upper crustal assimilation appears plausible in the generation. The interaction process was followed by the fractional crystallization of 29–32% plagioclase, 13–17% amphibole, 0.04–5% biotite and 3% Fe–Ti oxides during the rock evolution.

The MMEs in the plutons show identical mineralogical, chemical and isotopic composition relative to their host rocks. All geochemical characteristics, in conjunction with the isotopic ratios, indicate that the MMEs were most likely formed by the interaction processes between the lower crust-derived felsic and SCLM-derived mafic melts. Interaction process is evidenced by very similar isotopic ratios between enclaves and their host rocks, as is proposed by Holden et al. (1991) and Elburg (1996). Donaire et al. (2005), however, suggested a cognate origin based on the isotopic similarity. Actually, the MME data can provide valuable aspects with regard to the nature and role of the mantle-derived mafic magmas that involve in the construction of the hybrid granitoid rocks and also insights for the interaction processes between the mantle- and crust-derived magmas.

Acknowledgements

This work was supported by the Research Foundation of Karadeniz Technical University. Sincere thanks are due to the DAAD for scholarship to Orhan Karsli. He is most grateful to the Mineralogy Institute staff in Heidelberg, particularly Rainer Altherr and Hans-Peter Meyer for providing the microprobe studies and their great hospitality. Special thanks are due to M. Burhan Sadiklar for logistic support. The authors are also grateful to M. Cemal Göncüoğlu, Giampiero Poli and Bernard Bonin for their critical and constructive comments. We thank Ismet Gedik and Abdurrahman Dokuz for their comments on the geodynamic modeling of this study. Raif Kandemir and Ibrahim Uysal are thanked for their enthusiastic assistances during fieldwork. Teodosio Donaire and an anonymous reviewer are gratefully acknowledged for their comments resulting in a substantial improvement of an early draft.

References

Akin, H., 1979. Geologie, magmatismus und Lagerstattenbildung im ostpontischen Gebirge/Türkei aus der Sicht der Plattentektonik. Geol. Rundsch. 68, 253–283.

Altherr, R., Siebel, W., 2002. I-type plutonism in a continental back arc setting: Miocene granitoids and monzonites from the central Aegean Sea, Greece. Contrib. Mineral. Petrol. 143, 397–415.

Altherr, R., Henjes-Kunst, F., Langer, C., Otto, J., 2000. Interaction between crustal-derived felsic and mantle-derived mafic magmas in the Oberkirch Pluton (Eoropean Variscides, Schwarzwald, Germany). Contrib. Mineral. Petrol. 137, 304–322.

Aydin, F., Karsli, O., Sadiklar, M.B., 2003. Mineralogy and chemistry of biotites from eastern Pontide granitoid rocks, NE Turkey: some petrological implications for granitoid magmas. Chem. Erde-Geochem. 63, 163–182.

Barbarin, B., Didier, J., 1992. Genesis and evolution of mafic microgranular enclaves through various types of interaction between coexisting felsic and mafic magmas. Trans. R. Soc., Earth Sci. 83, 145–153.

Blundy, J.D., Holland, T.J.B., 1990. Calcic amphiboles equilibria and a new amphibole–plagioclase geothermometer. Contrib. Mineral. Petrol. 116, 433–447.

Boynton, W.V., 1984. Cosmochemistry of the rare earth elements: meteorite studies. In: Henderson, P. (Ed.), Rare Earth Element Geochemistry. Elsevier, Amsterdam, pp. 63–114.

Boztuğ, D., Jonckheere, R., Wagner, G.A., Yeğingil, Z., 2004. Slow Senonian and fast Paleocene–Early Eocene uplift of the granitoids in the Central Eastern Pontides, Turkey: apatite fission-track results. Tectonophysics 382, 213–228.

Boztuğ, D., Erçin, A.I., Kuruçelik, M.K., Göç, D., Kömür, I., Iskenderoğlu, A., 2006. Geochemical characteristics of the composite Kackar batholith generated in a Neo-Tethyan convergence system, eastern Pontides, Turkey. J. Asian Earth Sci. 27, 286–302.

Chappell, B.W., 1999. Aluminum saturation in I- and S-type granites and the characterization of fractionated hapogranites. Lithos 46, 531–551.

Chappell, B.W., White, A.J.R., 1992. I- and S-type granites in the Lachlan Fold Belt. Trans. R. Soc. Edinb. Earth Sci. 83, 1–26.

Chen, B., Arakawa, Y., 2005. Elemental and Nd–Sr isotopic geochemistry of granitoids from the West Jungar foldbelt (NW China), with implications for phanerozoic continental growth. Geochim. Cosmochim. Acta 69, 1307–1320.

Chen, J.F., Jahn, B.M., 1998. Crustal evolution of southeastern China: Nd and Sr isotopic evidence. Tectonophysics 284, 101–133.

Chen, B., Jahn, B.M., 2004. Genesis of post-collisional granitoids and basement nature of the Junggar Terrane, NW China: Nd–Sr isotope and trace element evidence. J. Asian Earth Sci. 23, 691–703.

Chen, B., Jahn, B.M., Wei, C., 2002. Petrogenesis of Mesozoic granitoids in the Dabie UHP complex, Central China: trace element and Nd–Sr isotope evidence. Lithos 60, 67–88.

Çakir, Ö., Erduran, M., 2004. Constraining crustal and uppermost mantle structure beneath station TBZ (Trabzon, Turkey) by receiver function and dispersion analyses. Geophys. J. Int. 158, 955–971.

Çakir, Ö., Erduran, M., Çınar, H., Yılmaztürk, A., 2000. Forward modelling receiver functions for crustal structure beneath station TBZ (Trabzon, Turkey). Geophys. J. Int. 140, 341–356.

De Paolo, D.J., 1981. Trace element and isotopic effects of combined wall-rock assimilation and fractional crystallization. Earth Planet. Sci. Lett. 53, 189–202.

Dokuz, A., Tanyolu, E., Genç, S., 2006. A mantle- and a lower crust-derived bimodal suite in the Yusufeli (Artvin) area, NE Turkey: trace element and REE evidence for subduction-related rift origin of Early Jurassic Demirkent intrusive complex. Intern. Earth Sci. 95, 370–394.

Donaire, T., Pascual, E., Pin, C., Duthou, J.L., 2005. Microgranular enclaves as evidence of rapid cooling in granitoid rocks: the case of the Los Pedroches granodiorite, Iberian Massif, Spain. Contrib. Mineral. Petrol. 149, 247–265.

Elburg, M.A., 1996. Evidence of isotopic equilibration between microgranitoid enclaves and host granodiorite, Warburton Granodiorite, Lachlan Fold Belt, Australia. Lithos 38, 1–22.

Elmas, A., 1995. Geology of the Kop Dağı area (Bayburt–Erzurum): evolution of a fore-arc basin (in Turkish). TPJD Bül. 6, 19–37.

Ferré, E.C., Bernard, E.L., 2001. geodynamic significance of early orogenic high-K crustal and mantle melts: example of the Corsica Batholith. Lithos 59, 47–67.

Frost, B.R., 1991. Introduction to oxygen fugacity and its petrologic importance. In: Lindsley, D.H. (Ed.), Oxide Minerals. Rev. Mineral, vol. 25. Mineralogical Society of America, pp. 1–9.

Frost, B.R., Mahood, G.A., 1987. Field, chemical and physical constraints on mafic–felsic interaction in the Lamarck granodioritem, Sierra Nevada, California. Geol. Soc. Amer. Bull. 99, 272–291.

Grove, T.L., Donnelly-Nolan, J.M., 1986. The evolution of young silisic lavas at Medicine lake Volcano, California: implications for the origin of compositional gaps in calc-alkaline series lavas. Contrib. Mineral. Petrol. 92, 281–302.

Grove, M., Harrison, T.M., 1996. ^{40}Ar diffusion in Fe-rich biotite. Am. Mineral. 81, 940–951.

Han, B.F., Wang, S.G., Jahn, B.M., Hong, D.W., Kagami, H., Sun, Y.L., 1997. Depleted mantle source for the Ulungur River A-type granites from North Xinjiang, China: geochemistry and Nd–Sr isotopic evidence and implications for Phanerozoic crustal growth. Chem. Geol. 138, 135–159.

Hawkesworth, C.J., Gallagher, K., Herot, J.M., McDermott, F., 1993. Mantle and slab contributions in arc magmas. Annu. Rev. Earth Planet. Sci. 21, 175–2004.

Hibbard, M.J., 1991. Textural anatomy of twelve magma-mixed granitoid systems. In: Didier, J., Barbarin, B. (Eds.), Enclaves and Granite Petrology. Develop. Petrol., vol. 13. Elsevier, Amsterdam, pp. 431–444.

Holden, P., Halliday, A.N., Stephens, W.E., 1987. Neodymium and strontium isotope content of microdiorite enclaves points to mantle input to granitoid production. Nature 330, 53–56.

Holden, P., Halliday, A.N., Stephens, W.E., Henney, P.J., 1991. Chemical and isotopic evidence for major mass transfer between mafic enclaves and felsic magma. Chem. Geol. 92, 135–152.

Hollanda, M.H.B.M., Pimentel, M.M., Jardim de Sa, E.F., 2003. Paleoproterozoic subduction-related metasomatic signatures in the lithospheric mantle beneath NE Brazil: inferences from trace element and Sr–Nd–Pb isotopic compositions of Neoproterozoic high-K igneous rocks. J. Am. Earth Sci. 15, 885–900.

Houseman, G.A., McKenzie, D.P., Molnar, P.J., 1981. Convective instability of a thickened boundary layer and its relevance for the thermal evolution of continental convergent belts. J. Geophys. Res. 86, 6115–6132.

Karsli, O., Aydin, F., Sadiklar, M.B., 2002. Geothermobarometric investigation of the Zigana Granitoid, eastern Pontides, Turkey. Int. Geol. Rev. 44, 277–286.

Karsli, O., Aydin, F., Sadiklar, M.B., 2004a. Magma interaction recorded in plagioclase zoning in granitoid systems, Zigana Granitoid, Eastern Pontides, Turkey. Turk. J. Eart. Sci. 13, 287–305.

Karsli, O., Aydin, F., Sadiklar, M.B., 2004b. The morphology and chemistry of K-feldspar megacrysts from İkizdere Pluton: evidence for acid and basic magma interactions in granitoid rocks, NE Turkey. Chem. Erde-Geochem. 64, 155–170.

Keskin, M., 2005. Domal Uplift and Volcanism in a Collision Zone without a Mantle Plume: evidence from Eastern Anatolia. http://www.mantleplumes.org/Anatolia.html.

Kumar, S., Rino, V., Pal, A.B., 2004. Field evidence of magma mixing from microgranular enclaves hosted in Palaeoproterozoic Malanjkhand granitoids, Central India. Gondwana Res. 7, 539–548.

Le Maitre, R.W., Bateman, P., Dudek, A., keller, J., Lameyre Le Bas, M.J., Sabine, P.A., Schmid, R., Sorensen, H., Streckeisen, A., Woolley, A.R., Zanettin, B., 1989. A Classification of Igneous Rocks and Glossary of Terms. Blackwell, Oxford.

Lopéz, S., Castro, A., 2001. Determination of the fluid-absent solidus and supersolidus phase relationships of MORB-derived amphibolites in the range 4–14 kbar. Am. Mineral. 86, 1396–1403.

Maniar, P.D., Piccoli, P.M., 1989. Tectonic discrimination of granitoids. Bull. Am. Geol. Soc. 101, 635–643.

Middlemost, E.A.K., 1994. Naming materials in the magma/igneous rock system. Earth-Sci. Rev. 37, 215–224.

Moore, W.J., McKee, E.H., Akinci, Ö., 1980. Chemistry and chronology of plutonic rocks in the Pontide Mountains, Northern Turkey. Symposium of European Copper Deposit, Belgrade, pp. 209–216.

Nittmann, J., Daccord, G., Stanley, H.E., 1985. Fractal growth of viscous fingers: quantitative characterization of a fluid instability phenomenon. Nature 314, 141–145.

Okay, A.I., Kelley, S.P., 1994. Tectonic setting, petrology and geochronology of jadeite+glaucophane and chloritoid+glacophane schists from north–west Turkey. J. Metamorph. Geol. 25, 743–746.

Okay, A.I., Şahintürk, Ö., 1997. Geology of the Eastern Pontides. In: Robinson, A.G. (Ed.), Regional and Petroleum Geology of the Black Sea and Surrounding Region. AAPG Memoir, vol. 68, pp. 292–311.

Okay, A.I., Şahintürk, Ö., Yakar, H., 1997. Stratigraphy and tectonics of the Pulur (Bayburt) region in the eastern Pontides. Miner. Res. Exp. Bull. 119, 1–24.

Parada, M.A., Nystrom, J.O., Levi, B., 1999. Multiple source for the Coastal Batholith of central Chile (31-340S): geochemical and Sr–Nd isotopic evidence and tectonic implications. Lithos 46, 505–521.

Peccerillo, A., Taylor, S.R., 1976. Geochemistry of Eocene calc-alkaline volcanic rocks from Kastamonu area, northern Turkey. Contrib. Mineral. Petrol. 58, 63–81.

Pedford, N., Gallagher, K., 2001. Partial melting of mafic (amphibolitic) lower crust by periodic influx of basaltic magma. Earth Planet. Sci. Lett. 193, 483–499.

Perugini, D., Poli, G., 2000. Chaotic dynamics and fractals in magmatic interaction processes: a different approach to the interpretation of mafic microgranular enclaves. Earth Planet. Sci. Lett. 175, 93–103.

Perugini, D., Poli, G., Christofides, G., Eleftheriadis, G., 2003. Magma mixing in the Sithonia Plutonic Complex, Greece: evidence from mafic microgranular enclaves. Mineral. Petrol. 78, 173–200.

Perugini, D., Ventura, G., Petrelli, M., Poli, G., 2004. Kinematic significance of morphological structures generated by mixing of magmas: a case study from Salina Island (southern Italy). Earth Planet. Sci. Lett. 222, 1051–1066.

Pin, C., Binon, M., Belin, J.M., Barbarin, B., Clemens, J.D., 1990. Origin of microgranular enclaves in granitoids: equivocal Sr–Nd evidence from Hercynian rocks in the Central France. J. Geophys. Res. 95, 17821–17828.

Poli, G.E., Tommasini, S., 1991. Model for the origin and significance of microgranular enclaves in calc-alkaline granitoids. J. Petrol. 32, 657–666.

Pouchou, J.L., Pichoir, F., 1985. "PAP" (ø.ρ.Z) correction procedure for improved quantitative microanalysis. In: Armstrong, J.T. (Ed.), Microbeam analysis. San Francisco Press, pp. 104–106.

Rapp, R.P., Watson, E.B., 1995. Dehydration melting of metabasalt at 8–32 kbar: implications for continental growth and crust–mantle recycling. J. Petrol. 36, 891–931.

Rapp, R.P., Watson, E.B., Miller, C.F., 1991. Partial melting of amphibolite/eclogite and the origin of Archean trondhjemites and tonalities. Precambrian Res. 51, 1–25.

Roberts, M.P., Clemens, J.D., 1993. Origin of high-potassium, calc-alkaline, I-type granitoids. Geology 21, 825–828.

Robinson, A.G., Banks, C.J., Rutherford, M.M., Hirst, J.P.P., 1995. Stratigraphic and structural development of the Eastern Pontides, Turkey. J. Geol. Soc. (Lond.) 152, 861–872.

Rottura, A., Bargossi, G.M., Caggianelli, A., Del Moro, A., Visona, D., Tranne, C.A., 1998. Origin and significance of the Permian high-K calc-alkaline magmatism in the central-eastern Southern Alps, Italy. Lithos 45, 329–348.

Rudnick, R.L., McDonough, W.F., McCulloch, M.T., Taylor, S.R., 1986. Lower crustal xenoliths from Queensland, Australia: evidence for deep crustal assimilation and fractionation of continental basalts. Geochim. Cosmochim. Acta 50, 1099–1115.

Rushmer, T., 1991. Partial melting of two amphibolites: contrasting experimental results under fluid-absent conditions. Contrib. Mineral. Petrol. 107, 41–59.

Şahin, S.Y., Güngör, Y., Boztuğ, D., 2004. Comparative petrogenetic investigation of composite Kaçkar Batholith granitoids in Eastern Pontide magmatic arc-Northern Turkey. Earth Planets Space 56, 429–446.

Schmidt, M.W., 1992. Amphibole composition in tonalities as a function of pressure: an experimental calibration of the Al-in-hornblende barometer. Contrib. Mineral. Petrol. 110, 304–310.

Şen, C., Dunn, T., 1994. Dehydration melting of a basaltic composition amphibolite at 1.5 and 2.0 GPa: implications for the origin of adakites. Contrib. Mineral. Petrol. 117, 394–409.

Şen, C., Arslan, M., Van, A., 1998. Geochemical and petrological characteristics of the Eastern Pontide Eocene (?) alkaline volcanic province, NE Turkey. Turk. J. Eart. Sci. 7, 231–239.

Şengör, A.M.C., Yilmaz, Y., 1981. Tethyan evolution of Turkey: a plate tectonic approach. Tectonophysics 75, 181–241.

Şengör, A.M.C., Özeren, S., Genç, T., Zor, E., 2003. East Anatolian high plateau as a mantle-supported, North–south shortened domal structure. Geophys. Res. Lett. 30 (24), 8045. doi:10.1029/2003GL017858.

Soesoo, A., 2000. Fractional crystallization of mantle-derived melts as a mechanism for some I-type granite petrogenesis: an example from Lachlan Fold Belt, Australia. J. Geol. Soc. 157, 135–149.

Spencer, K.J., Lindsley, D.H., 1981. A solution model for coexisting iron–titanium oxides. Am. Mineral. 66, 1189–1201.

Steiger, R.H., Jäger, E., 1977. Subcommission on geochronology: convention on the use of decay constants in geo- and cosmochronology. Earth Planet. Sci. Lett. 36, 359–362.

Streckeisen, A., 1976. To each plutonic rock its proper name. Earth-Sci. Rev. 12, 1–33.

Sun, S.S., McDonough, W.E., 1989. Chemical and isotopic systematics of oceanic basalts: implications for mantle composition an processes. In: Saunders, A.D., Norry, M.J. (Eds.), Magmatism in the Ocean Basins. Special Publication. Geological Society of London, pp. 313–345.

Taner, M.F., 1977. Etuda geologique et petrographique de la region de Güneyce-İkizdere, situee au sud de Rize (Pontides orientalas, Turquie). PhD Thesis, (unpublished), Universite de Geneve, 180 pp.

Tepper, J.H., Nelson, B.K., Bergantz, G.W., Irving, A.J., 1993. Petrology of the Chilliwack batholith, North Cascades, Washington: generation of calc-alkaline granitoids by melting of mafic lower crust with variable fugacity. Contrib. Mineral. Petrol. 113, 333–351.

Thirlwall, M.F., Jones, N.W., 1993. Isotope geochemistry and contamination mechanism of Tertiary lavas from Skye, northwest Scotland. In: Hawkesworth, C.J., Norry, M.J. (Eds.), Continental Basalts and Mantle Xenoliths. Shiva, Cheshire, pp. 186–208.

Tokel, S., 1977. Doğu Karadeniz Bölgesinde Eosen yaþlı kalk-alkalen andezitler ve jeotektonizma. Türk. Jeol. Bül. 20, 49–54.

Topuz, G., Altherr, R., Schwarz, W.H., Siebel, W., Satir, M., Dokuz, A., 2005. Post-collisional plutonism with adakite-like signatures: the Eocene Saraycik granodiorite (Eastern Pontides, Turkey). Contrib. Mineral. Petrol. 150, 441–455.

Turner, S.P., Foden, J.D., Morrison, R.S., 1992. Derivation of some A-type magmas by fractionation of basaltic magma; an example from the Padthaway Ridge, South Australia. Lithos 28, 151–179.

Vernon, R.H., 1984. Microgranitoid enclaves in granites-globules of hybrid magma quenched in a plutonic environment. Nature 309, 438–439.

Vernon, R.H., 1990. Crystallization and hybridism in microgranitoid enclave magmas: microstructural evidence. J. Geophys. Res. 95, 17849–17859.

Volkert, R.A., Feigenson, M.D., Patino, L.C., Delaney, J.S., Drake Jr., A.A., 2000. Sr and Nd isotopic compositions, age and petrogenesis of A-type granitoids of the Vernon Supersuite, New Jersey Highlands, USA. Lithos 50, 325–347.

Waight, T.E., Maas, R., Nicholls, I.A., 2000. Fingerprinting feldspar phenocrysts using crystal isotopic composition stratigraphy: implications for crystal and magma mingling in S-type granites. Contrib. Mineral. Petrol. 139, 227–239.

Weinberg, R.F., Sial, A.N., Pessoa, R.R., 2001. Magma flow within the travers pluton, northeastern Brazil: compositional and thermal convection. Geol. Soc. Amer. Bull. 113, 508–520.

Wiebe, R.A., 1991. Commingling of contrasted magmas and generation of mafik enclaves in granitic rocks. In: Didier, J., Barbarin, B. (Eds.), Enclaves and Granite Petrology. Dev. Petrol., vol. 13, pp. 393–402.

Wiebe, R.A., 1996. Mafic–silisic layered intrusions: the role of basaltic injections on magmatic processes and evolution of silisic magma chambers. Trans. R. Soc. Edinb. Earth Sci. 87, 233–242.

Wiebe, R.A., Smith, D., Sturm, M., King, E.M., Seckler, M.S., 1997. Enclaves in the Cadillac Mountain Granite (Coasta Maine) samples of hybrid magma the base of the chamber. J. Petrol. 38, 393–423.

Winther, K.T., 1996. An experimentally based model for the origin of tonalitic and trondhjemitic melts. Chem. Geol. 127, 43–59.

Wolf, M.B., Wyllie, P.J., 1994. Dehydration-melting of amphibolite at 10 kbar: the effects of temperature and time. Contrib. Mineral. Petrol. 115, 369–383.

Wyllie, P.J., Wolf, M.B., 1993. Amphibolite dehydration-melting: sorting out the solidus. In: Prichard, H.M., Alabaster, T., Harris, N.B.W., Neary, C.R. (Eds.), Magmatic Processes and Plate Tectonics. Geol. Soc. Spec. Publ., vol. 76, pp. 405–416.

Yilmaz, Y., 1972. Petrology and structure of the Gümüşhane granite and the surrounding rocks. NE Anatolia, PhD Thesis University College London, England. 248 pp.

Yilmaz, S., Boztuğ, D., 1996. Space and time relations of three plutonic phases in the Eastern Pontides, Turkey. Int. Geol. Rev. 38, 935–956.

Yilmaz, Y., Tüysüz, O., Yiğitbaþ, E., Genç, Ş.C., Şengör, A.M.C., 1997. Geology and tectonic evolution of the Pontides. In: Robinson, A.G. (Ed.), Regional and Petroleum Geology of the Black Sea and Surrounding Region. Am. Assoc. Petrol. Geol. Mem., vol. 68, pp. 183–226.

Zindler, A., Hart, S.R., 1986. Chemical geodynamics. Annu. Rev. Earth Planet. Sci. 14, 493–571.